Title: The fate of carbon in a mature forest under carbon dioxide enrichment

M. Jiang[1], B.E. Medlyn[1], J.E. Drake[1,2], R.A. Duursma[1], I.C. Anderson[1], C.V.M. Barton[1], M.M. Boer[1], Y. Carrillo[1], L.Castañeda-Gómez[1], L. Collins[1,3,4], K.Y. Crous[1], M.G. De Kauwe[5,6,7], B.M. dos Santos[8,9], K.M. Emmerson[10], S.L. Facey[1], A.N. Gherlenda[1], T.E. Gimeno[1,11,12], S. Hasegawa[1,13], S.N. Johnson[1], C.A. Macdonald[1], K. Mahmud[1,14], A. Kännaste[15], B.D. Moore[1], L. Nazaries[1], E.H.J. Neilson[8,9], U.N. Nielsen[1], Ü. Niinemets[15], N.J. Noh[1,16], R. Ochoa-Hueso[1,17], V.S. Pathare[1,18], E. Pendall[1], J. Pihlblad[1], J. Pineiro[1,19], J.R. Powell[1], S.A. Power[1], P.B. Reich[1,20], A.A. Renchon[1], M. Riegler[1], R. Rinnan[21], P. Rymer[1], R.L. Salomón[22], B.K. Singh[1,23], B. Smith[1,24], M.G. Tjoelker[1], J.K.M. Walker[1], A. Wujeska-Klause[1], J. Yang[1], S. Zaehle[25], and D.S. Ellsworth[1]

Affiliation:

[1]Hawkesbury Institute for the Environment, Western Sydney University, Locked Bag 1797, Penrith, NSW, 2751, Australia

[2]Department of Sustainable Resources Management, College of Environmental Science and Forestry, State University of New York, Syracuse, NY 13210, USA

[3]Department of Ecology, Environment and Evolution, La Trobe University, Bundoora, VIC 3086, Australia

[4]Arthur Rylah Institute for Environmental Research, Department of Environment, Land, Water and Planning, PO Box 137, Heidelberg, VIC 3084, Australia

[5]ARC Centre of Excellence for Climate Extremes, University of New South Wales, Sydney, NSW 2052, Australia

[6]Climate Change Research Centre, University of New South Wales, Sydney, NSW, 2052, Australia

[7]Evolution and Ecology Research Centre, University of New South Wales, Sydney, NSW, 2052, Australia

[8]Plant Biochemistry Laboratory, Department of Plant and Environmental Sciences, University of Copenhagen, Thorvaldsensvej 40, 1871 Frederiksberg C, Copenhagen, Denmark

[9]VILLUM Research Center for Plant Plasticity, University of Copenhagen, Thorvaldsensvej 40, 1871 Frederiksberg C, Copenhagen, Denmark

[10]Climate Science Centre, CSIRO Oceans & Atmosphere, Aspendale, VIC 3195, Australia

[11]Basque Centre for Climate Change, Leioa, 48940, Spain

[12]Ikerbasque, Basque Foundation for Science, 48008 Bilbao, Spain

[13]Department of Forest Ecology and Management, Swedish University of Agricultural Sciences (SLU), Umeå, SE-90183, Sweden

[14]Department of Geography, Indiana University, Bloomington, IN 47405, USA

[15]Estonian University of Life Sciences, Kreutzwaldi 1, 51006, Tartu, Estonia

[16]Forest Technology and Management Research Center, National Institute of Forest Science, Gyeonggi-do, 1186, Korea

[17]Department of Biology, IVAGRO, University of Cádiz, Campus de Excelencia Internacional Agroalimentario (CeiA3), Campus del Rio San Pedro, 11510 Puerto Real, Cádiz, Spain

[18]School of Biological Sciences, Post Office Box 646340, Washington State University, Pullman, WA 99164-6340, USA

[19]Division of Plant and Soil Sciences, West Virginia University, Morgantown, WV, USA

[20]Department of Forest Resources, University of Minnesota, St Paul, Minnesota, 55108, USA

[21]Terrestrial Ecology Section, Department of Biology, University of Copenhagen, Universitetsparken 15, DK-2100, Copenhagen, Denmark

[22]Laboratory of Plant Ecology, Faculty of Bioscience Engineering, Ghent University, Coupure links 653, 9000 Ghent, Belgium

[23]Global Centre for Land Based Innovation, Western Sydney University, Building L9, Locked Bag 1797, Penrith South, NSW, 2751, Australia

[24]Department of Physical Geography and Ecosystem Science, Lund University, 22362, Lund, Sweden

[25]Max Planck Institute for Biogeochemistry, Hans-Knöll-Str. 10, 07745 Jena, Germany

Abstract

Atmospheric carbon dioxide enrichment (eCO_2) can enhance plant carbon uptake and growth[1,2,3,4,5], thereby providing an important negative feedback to climate change by slowing the rate of increase of the atmospheric CO_2 concentration[6]. While evidence gathered from young aggrading forests has generally indicated a strong CO_2 fertilization effect on biomass growth[3,4,5], it is unclear whether mature forests respond to eCO_2 in a similar way. In mature trees and forest stands[7,8,9,10], photosynthetic uptake has been found to increase under eCO_2 without any apparent accompanying growth response, leaving an open question about the fate of additional carbon fixed under eCO_2[4,5,7,8,9,10,11]. Here, using data from the first ecosystem-scale Free-Air CO_2 Enrichment (FACE) experiment in a mature forest, we constructed a comprehensive ecosystem carbon budget to track the fate of carbon as the forest responds to four years of eCO_2 exposure. We show that, although the eCO_2 treatment of ambient +150 ppm (+38%) induced a 12% (+247 g C m^{-2} yr^{-1}) increase in carbon uptake through gross primary production, this additional carbon uptake did not lead to increased carbon sequestration at the ecosystem level. Instead, the majority of the extra carbon was emitted back into the atmosphere via several respiratory fluxes, with increased soil respiration alone accounting for ~50% of the total uptake surplus. Our results call into question the predominant thinking that the capacity of forests to act as carbon sinks will be generally enhanced under eCO_2, and challenge the efficacy of climate mitigation strategies that rely on ubiquitous CO_2 fertilization as a driver of increased carbon sinks in global forests.

Main text

Globally, forests act as a large carbon sink, absorbing a significant portion of the anthropogenic CO_2 emissions[1,12], an ecosystem service that has tremendous social and

economic value. Whether mature forests will remain carbon sinks into the future is of critical importance for aspirations to limit climate warming to no more than 1.5 °C above pre-industrial levels[13]. Free-Air CO_2 Enrichment (FACE) experiments provide an opportunity to determine the capacity of ecosystems to sequester carbon under the higher atmospheric CO_2 concentrations expected in the future[3,4,5,7,8,10,11]. Evidence gathered from the four first-generation forest FACE experiments, which all measured responses of rapidly-growing young forest plantations, has generally indicated a strong CO_2 fertilization effect on biomass growth[3,4]. This CO_2 fertilization effect has been hypothesized to be one of the largest drivers of the terrestrial carbon sink and its acceleration in recent decades[14], potentially accounting for up to 60% of present-day terrestrial carbon sequestration[2]. However, younger trees are generally more responsive to rising CO_2 than mature trees[11], potentially because nutrient limitation increases with stand age[15]. Thus, extrapolating evidence collected from these experiments may be argued to provide an upper limit on how much carbon can be stored by global forests under eCO_2[16]. Evidence from experiments with older trees on nutrient-poor soils suggests that although eCO_2 increases leaf photosynthesis to a similar degree as in young forests, stimulation of biomass growth and carbon storage may be lower or absent[7,8,9,10]. Reconciling these conflicting observations is a crucial step towards quantifying the carbon sequestration capacity of mature forests in the future. It requires that we identify the fate of the extra carbon fixed under eCO_2 in mature forests, which are expected to be closer to a state of equilibrium between carbon uptake and turnover, compared to young aggrading stands.

The *Eucalyptus* FACE (EucFACE) experiment is the world's first replicated, ecosystem-scale mature forest FACE experiment (Extended Data Figure 1, 2). It is located in a warm-temperate evergreen forest that has remained undisturbed for the past 90 years, is dominated

105 by the regionally widespread tree *Eucalyptus tereticornis* and has an understorey composed
106 principally of native grasses and shrubs. The low-fertility soil has been shown to limit tree
107 growth in an adjacent phosphorus-fertilization experiment[17]. Seven ecosystem-scale models
108 were used to predict the eCO_2 response at EucFACE in advance of the experiment[18],
109 highlighting three alternative hypotheses for the expected ecosystem response based on
110 plausible assumptions incorporated in different models[19]. These hypotheses were: (i)
111 enhanced photosynthesis under eCO_2 would lead to increased biomass accumulation; (ii)
112 eCO_2-induced increase in photosynthesis would be directly down-regulated by limited
113 nutrient availability; or (iii) eCO_2-induced increase in photosynthesis would lead to increased
114 autotrophic respiration[18]. This range of predictions among a suite of well-tested models
115 indicated a prognostic knowledge gap as to how the carbon cycling of mature forests would
116 respond to the expected rise in atmospheric CO_2 concentration[11], which is crucial to resolve in
117 the face of future carbon-climate uncertainty[20].
118
119 To date, both canopy trees and understorey plants at EucFACE have shown increased rates of
120 leaf photosynthesis but the canopy trees showed no significant increase in aboveground
121 biomass growth under eCO_2[7], reflecting a similar lack of response observed in other eCO_2
122 experiments on mature trees[8,9,10]. Incorporating leaf-scale gas exchange measurements into a
123 process-based tree stand model, it was estimated that the observed +19% stimulation of light-
124 saturated overstorey leaf photosynthesis[7] corresponded to a +11% stimulation of whole-
125 canopy gross primary production (GPP) in response to eCO_2[21]. However, the probable fate of
126 the extra carbon fixed under eCO_2 remained undetermined. Where did the extra carbon go?
127
128 To answer this question, we compiled measurements on all major carbon pools and fluxes
129 collected over four years of experimental treatment (2013-2016), including individual and

aggregated biomass and associated fluxes measured or inferred from plants, litter, soil, microbes, and insects, and constructed an ecosystem carbon budget (Figure 1) under both ambient (aCO_2) and eCO_2 conditions (+150 ppm). We first confirmed mass balance of the ecosystem carbon budget by checking agreement between independent estimates of GPP and soil respiration (R_{soil}) derived from separate data streams (Extended Data Figure 3; see Methods). For GPP of the aCO_2 plots, we confirmed that a process-based model estimate of overstorey and understorey GPP (2059 ± 211 g C m^{-2} yr^{-1}), driven by site-specific meteorology and treatment-specific physiological data, broadly agreed with the sum of data-driven estimates of net primary production (NPP) and autotrophic respiration (2068 ± 61 g C m^{-2} yr^{-1}). The carbon-use efficiency (NPP/GPP) of this mature forest was estimated to be 0.31 ± 0.03, which is on the low end of global forest estimates, but consistent with studies that have observed this ratio to decline with stand age[22] (Extended Data Figure 2). We further confirmed carbon mass balance for R_{soil} of the aCO_2 plots by comparing soil chamber-based estimates (1097 ± 86 g C m^{-2} yr^{-1}) with the sum of litterfall and independently estimated root respiration (1086 ± 14 g C m^{-2} yr^{-1}), assuming no change in soil carbon pool (see Methods). This agreement between independent estimates of components of the ecosystem carbon budget gives confidence that our measurements captured the pools and fluxes of carbon with low aggregate uncertainty and hence allow us to infer the fate of the extra carbon fixed under eCO_2.

To accommodate the inherent pre-treatment plot differences (see Methods), we normalized the CO_2 responses across plots by using a linear mixed-model with plot-specific pre-treatment leaf area index as a covariate[23,24]. The non-normalized eCO_2 responses are provided in Extended Data Figure 4, and generally confirm the findings but with larger uncertainty. Our normalized responses (Figure 2, Extended Data Figure 5) showed that eCO_2 induced an

155 average of 12% increase (+247 ± 195 g C m^{-2} yr^{-1}, mean ± one standard deviation) in carbon
156 uptake, including contributions of overstorey (+192 ± 193 g C m^{-2} yr^{-1}) and understorey GPP
157 (+55 ± 21 g C m^{-2} yr^{-1}). The fate of this additional carbon entering the system under eCO_2
158 was primarily traced to an increase in R_{soil} (+128.8 ± 116.7 g C m^{-2} yr^{-1}, or 52% of the carbon
159 uptake surplus), followed by a smaller increase in tree stem respiration (R_{stem}; +40.0 ± 43.6 g
160 C m^{-2} yr^{-1}, or 16% of the carbon uptake surplus). In comparison, the increase in total NPP
161 (+67.3 ± 12.7 g C m^{-2} yr^{-1}, or 28% of the carbon uptake surplus) corresponded to a smaller
162 increase in storage of the total carbon pools at the ecosystem-level (ΔC_{pools}; +31.6 ± 188.8 g C
163 m^{-2} yr^{-1}, or 12.8% of the carbon uptake surplus, Extended Data Figure 6). There was thus
164 little evidence of additional carbon accumulation under eCO_2 in this mature forest ecosystem.
165 We then compared three alternative methods (see Methods) of estimating net ecosystem
166 production (NEP; Figure 3). All three indicated that the ecosystem remained close to carbon-
167 neutral under ambient CO_2 over the experimental period (mean ± SD for the methods: 28 ±
168 225, 21 ± 129, -73 ± 50 g C m^{-2} yr^{-1}, respectively), and that eCO_2 of +150 ppm did not result
169 in statistically significant increases in ecosystem carbon storage (109 ± 258, -19 ± 171, -42 ±
170 262 g C m^{-2} yr^{-1}, respectively). However, the variability reported here means that we cannot
171 fully rule out the possibility of additional carbon storage under eCO_2, but we stress that our
172 individual and aggregated responses consistently suggest a lack of CO_2 response in this
173 mature forest (Figure 2 & 3, Extended Data Figure 5).
174
175 The relatively small but positive NPP response to eCO_2 was mainly driven by the understorey
176 aboveground NPP response (NPP_{ua}; +50.3 ± 17.9 g C m^{-2} yr^{-1}), which was 75% of the net
177 NPP response (Figure 2). However, this significant NPP_{ua} response did not result in an
178 equivalent eCO_2 effect on understorey aboveground biomass increment (+27.2 ± 29.7 g C m^{-2}
179 yr^{-1}), suggesting a possible higher understorey biomass turnover under eCO_2. Smaller fluxes,

often neglected in other ecosystem carbon budgets, such as leaf consumption by insect herbivores (NPP_{ins}; 25.5 ± 4.3 vs. 27.8 ± 6.3 g C m^{-2} yr^{-1}, aCO_2 vs. eCO_2 mean ± SD), insect frass production (Frass; 10.5 ± 1.8 vs. 11.4 ± 2.6 g C m^{-2} yr^{-1}), vegetation volatile carbon emission (VC; 2.63 ± 0.18 vs. 2.45 ± 0.13 g C m^{-2} yr^{-1}), net ecosystem methane uptake (CH_4; 0.18 ± 0.0009 vs. 0.19 ± 0.0003 g C m^{-2} yr^{-1}), and leaching of dissolved organic carbon (DOC; 0.16 ± 0.017 vs. 0.17 ± 0.024 g C m^{-2} yr^{-1}), contributed to the closure of the overall ecosystem carbon budget (Figure 1; Extended Data Figure 3), but were not quantitatively important in explaining pathways of the carbon uptake surplus under eCO_2 (Figure 2, Extended Data Figure 5, Extended Data Figure 6).

Here we provide some of the first replicated experimental evidence on the probable fate of carbon under eCO_2 in intact mature forest. We found that increased R_{soil} accounted for ~50% of the extra photosynthate produced by plants under eCO_2. It has been suggested that the increase in R_{soil} at EucFACE was likely a consequence of increased root and rhizosphere respiration[25,26], in contrast to other FACE sites where increased R_{soil} was attributed to enhanced soil organic matter decomposition (e.g. DukeFACE[27]). Here, the eCO_2-induced increase in R_{soil} was not accompanied by substantial changes in root respiration (18.6 ± 20.1 g C m^{-2} yr^{-1}) or in carbon pools associated with fine roots (+7.0 ± 12.5 g C m^{-2} yr^{-1}), microbes (+1.9 ± 3.5 g C m^{-2} yr^{-1}), mycorrhizae (+0.4 ± 0.5 g C m^{-2} yr^{-1}), leaf litter (+27.1 ± 38.6 g C m^{-2} yr^{-1}) or soil (-23.8 ± 159.6 g C m^{-2} yr^{-1}), suggesting that the additional carbon fixed under eCO_2 may have led to an enhanced carbon transport belowground and a rapid belowground turnover of this flux. Assimilation of these data into a carbon balance model supports this inference (Extended Data Figure 7, see Methods for details). An initial enhancement in nitrogen and phosphorus mineralization was observed[28], which suggested that the increased R_{soil} with eCO_2 could reflect soil organic matter priming with the potential to alleviate plant

205 nutrient stress in this low-phosphorus soil[28,29]. However, the enhanced soil mineralization rate
206 and associated increase in nutrient availability did not persist over time[28], indicating that this
207 increased belowground carbon allocation and the rapid turnover of this flux was not effective
208 in increasing phosphorus availability to the plants[30].
209
210 The ecosystem carbon budget presented here provides an opportunity to confront the three
211 alternative hypotheses of the response of this system to eCO_2 treatment that emerged from
212 model predictions made in advance of the experiment[18]. Our data do not support any of the
213 three hypotheses. The eCO_2-induced increase in photosynthesis was not strongly down-
214 regulated by low nutrient availability[7,21]; nor did the eCO_2-induced additional carbon uptake
215 lead to additional biomass accumulation, or enhanced aboveground respiration. These
216 predictions reflect common mechanisms by which terrestrial vegetation models implement
217 nutrient limitation of the eCO_2 response[18,19,31,32]. In contrast, our results suggest a direct
218 connection between plant photosynthesis and belowground activity (Extended Data Figure 7),
219 in which increased belowground carbon allocation increased soil respiration at a rate that
220 accounted for half of the extra carbon fixed under eCO_2 (Figure 2). Predictions made in
221 advance of the experiment did not capture this additional belowground carbon flux, despite
222 their general agreement with data on turnover rates of major carbon pools (Extended Data
223 Figure 8). This increased soil respiration has been demonstrated by some models to be an
224 important and often overlooked mechanism that reduces global soil carbon sequestration
225 relative to estimates by many current models[33]. As a consequence of including this rapid
226 turnover of the increased belowground carbon allocation in terrestrial biosphere models, the
227 time-lag in emitting some of the extra carbon via biomass accumulation and litterfall input
228 into the soils may be reduced, thereby leading to faster cycling of carbon[34] and therefore
229 possible different trajectories of carbon-climate predictions for the future.

A major form of land-based climate mitigation actions envisaged in the 2015 Paris Agreement is to enhance forest biomass carbon stocks globally through the protection of existing, largely mature, forests, and through afforestation of new areas. The mitigation potential of forests lies in the accumulated stock of ecosystem carbon, not in the short-term rate of forest photosynthesis. The probable fate of additional carbon determined in our study (Figure 2) challenges the current thinking that all non-aggrading mature forests will contribute to enhanced carbon sinks due to CO_2 fertilization[35], which further questions the allowable CO_2 emission targets sourced from existing carbon cycle models[13,36]. Given that the effect of CO_2 fertilization may be one of diminishing returns over time[14], the statistically non-significant eCO_2 effect on NEP (Figure 3), if representative of nutrient-limited mature forest ecosystems generally, suggests an even weaker carbon sink in the future, especially in low-phosphorus systems such as EucFACE. Future research efforts should target a deeper understanding of the nutrient-carbon feedbacks that likely constrain the carbon sink potential of mature forests under eCO_2, and evaluate the implications of a potentially weaker terrestrial land carbon sink in the development of robust mitigation strategies in the face of climate change. More importantly, whilst the terrestrial carbon sink is integral to current strategies for climate change mitigation, our results call for more active reductions of anthropogenic emissions to meet the targets of the Paris Agreement.

Methods

EucFACE site description

The EucFACE facility (Extended Data Figure 1) is located in a mature evergreen *Eucalyptus* forest on an alluvial spodosol in western Sydney, Australia (33°36'S, 150°44'E). The site has been a remnant patch of native Cumberland Plain woodland since the 1880's and has remained unmanaged for at least the past 90 years, with *Eucalyptus tereticornis* Sm. as the dominant tree species (98% of the overstorey basal area). *Eucalyptus* trees occur naturally across Australia, accounting for 78% of native forest area in Australia[37] and are planted widely around the globe[38]. Infrastructure for six large circular plots (490 m^2 each) was established in 2010. Starting on 18th September 2012, three plots were subjected to free-air CO_2 enrichment treatment using a computer-controlled pre-dilution method. The CO_2 concentrations at EucFACE were ramped up over a six-month period, increasing by +30 ppm every five weeks in discrete steps (+30, 60, 90, 120, and 150 ppm). The full elevated CO_2 treatment of +150 ppm started on 6th February 2013 during daylight hours over all days of the year. The site is characterized by a humid temperate-subtropical transitional climate with a mean annual temperature of 17.5°C and a mean annual precipitation of 800 mm (Figure S1). The soil is a Holocene alluvial soil of low fertility with low phosphorus content[7,17]. Soil texture is a loamy sand (> 75% sand content) up to 50 cm in depth. From ca. 50 to 300 cm depth, soils are sandy clay loam, with > 30% silt and clay. Average bulk density is 1.39, 1.69 and 1.71 g cm^{-3} for depths of 0-10, 10-20 and 20-30 cm, respectively (Figure S2). Permanent groundwater depth is ~11 m below the soil surface[39]. Understorey vegetation is a diverse mixture of 86 species including forbs, graminoids and shrubs[40]. The dominant understorey species is *Microlaena stipoides*, a C_3 perennial grass that accounted for ~70% of herbaceous biomass and responded rapidly to rainfall variability[41].

Estimates of carbon pools and fluxes

We estimated plot-specific carbon pools and fluxes at EucFACE over 2013-2016 (Extended Data Table 1). We defined pools as a carbon reservoir and annual increments as the annual changes in the size of each reservoir. We compartmentalized the ecosystem into 11 carbon pools, namely overstorey leaf (C_{ol}), stem (C_{stem}), fine root (C_{froot}), coarse root (C_{croot}), intermediate root (C_{iroot}), understorey aboveground (C_{ua}), soil (C_{soil}), microbe (C_{micr}), mycorrhizae (C_{myco}), leaf litter (C_{lit}), and aboveground insect (C_{ins}) carbon pools, and reported pool size in the unit of g C m^{-2}. We defined fluxes as components of the carbon flow through the system, and report them in the unit of g C m^{-2} yr^{-1}. All annual incremental changes in carbon pools were reported in g C m^{-2} yr^{-1} with a symbol Δ. We converted estimates of biomass into carbon content using variable-specific carbon fractions (*f*) defined in Extended Data Table 2. Below we describe how each pool and flux was estimated.

Pools

Soil carbon pool (C_{soil}; Figure S2**)** was estimated based on quarterly sampled soil carbon content (oven-dried at 40 °C for 48 hours) and plot-specific soil bulk density at three depths (0 - 10 cm, 10 - 20 cm, 20 - 30 cm). Out of the 15 dates when samples were taken, soil carbon content below the top 10 cm of soil was measured on three dates. To obtain a more accurate estimate of annual incremental change in soil carbon pool, we therefore reported soil carbon pool for the top 10 cm only. There were no temporal and eCO_2 trends in soil carbon content at deeper depths.

296 **Overstorey leaf carbon pool (C_{ol};** Figure S3**)** was estimated based on continuous measures
297 of leaf area index (LAI) and specific leaf area (SLA, m^2 leaf area g^{-1} leaf DM), following C_{ol}
298 = LAI × SLA × f_{ol}, where f_{ol} is a carbon fraction constant for overstorey leaves (Extended
299 Data Table 2). Daily averages of plot-specific LAI were estimated based on the attenuation of
300 diffuse radiation in a homogenous canopy[24]. The number of observations varies between days,
301 depending on the number of 30-minute cloudy periods. SLA was estimated based on time-
302 series measures of leaf mass per area (LMA), and was then linearly interpolated to plot-
303 specific daily values over time.
304
305 **Stem carbon pool (C_{stem};** Figure S4**)** was estimated based on tree-specific height and
306 diameter at breast height (DBH) measurements, and an allometric scaling relationship derived
307 for *E. tereticornis*[7,42]. DBH changes were measured repeatedly at roughly monthly intervals,
308 at 1.3 m height. Bark was periodically removed from under the dendrometer bands - this
309 effect on DBH was considered by calculating biomass once per year using December data
310 only. Stem biomass data were summed for each plot and averaged over the plot area to obtain
311 ground-based estimates, and was then converted into C_{stem} using treatment-specific carbon
312 fraction (Extended Data Table 2).
313
314 **Understorey aboveground carbon pool (C_{ua}**; Figure S5**)** was estimated at 1-3 month
315 intervals between February 2015 and December 2016 using non-destructive measurements of
316 plant height obtained from stereo-photography[43]. In each of the four 2m × 2m understorey
317 monitoring subplots within each plot, stereo photographs were collected using a Bumblebee
318 XB3 stereo camera (Point Grey Research) mounted ~2.4 m above the ground surface and
319 facing vertically downwards towards the center of the subplot. Stereo images were taken at
320 dusk under diffuse light conditions to avoid measurement errors related to shadows from

trees and EucFACE infrastructure. On each sampling date, three sets of stereo photographs were taken in each subplot to produce a large number (i.e. 100,000 s) of understorey plant height estimates from which mean plant height (H_{mean}, in m) was calculated for each plot. Understorey aboveground biomass (B_{ua}, in kg m^{-2}) for each plot was predicted from H_{mean} using an empirical model developed for the grassy understorey vegetation at EucFACE ($B_{ua} = 1.72 \times H_{mean} - 0.05$)[43]. The four subplot-level estimates were averaged to obtain a plot-level estimate of B_{ua}, and then converted to an estimate of C_{ua} using a carbon fraction constant (Extended Data Table 2).

Root carbon pool (C_{root}) consists of fine root (C_{froot}), intermediate root (C_{iroot}), and coarse root (C_{croot}) pools, with C_{froot} defined as roots with diameter of < 2 mm, C_{iroot} defined as roots with diameter of 2 – 3 mm, and the remaining roots defined as C_{croot} (Figure S6). The C_{root} pool includes roots of both overstorey and understorey vegetation. Total root biomass (B_{root}) was estimated based on an allometric relationship with stand basal area (derived from DBH) derived for Australian forest species[44], as follows: $\ln(B_{root}) = 0.787 \times \ln(DBH) + 1.218$.

Standing intermediate root (2-3 mm in diameter) and fine root biomass (< 2 mm in diameter) were sampled in four subplots per plot at two depths (0 – 10 cm and 10 – 30 cm) in year 2017, whereas only fine root biomass at the same depths with the same number of subplots was repeatedly sampled over the period of 2014-2016[29]. We estimated a depth-specific relationship between fine root biomass (< 2 mm in diameter) and total root biomass less than 3 mm in diameter based on samples collected in 2017, and calculated the intermediate root biomass for the period of 2014-2016 based on its corresponding fine root biomass. Coarse root biomass was then estimated as the net difference between total allometrically-derived root biomass and that of roots with diameter < 3mm. The fine, intermediate, and coarse root

346 biomass were multiplied by the corresponding carbon fraction constants to obtain C_{froot}, C_{iroot},
347 and C_{croot}, respectively (Extended Data Table 2).
348
349 **Microbial carbon pool (C_{micr})** was estimated based on fumigation extraction and 0.5 M
350 K_2SO_4 extraction as in Ref. 25 using samples taken at 0-10 cm soil depth over the period of
351 2012 - 2015. Total organic carbon was determined on a Shimadzu TOC analyzer (TOC-L
352 TNM-L; Shimadzu, Sydney, Australia), which was then multiplied by soil bulk density over
353 the same soil depth to obtain the C_{micr} (Figure S7a).
354
355 **Mycorrhizal carbon pool (C_{myco})** for the top 10 cm of soil was estimated via measurements
356 of colonization of mycorrhizal in-growth bags, carbon isotopic partitioning, microbial
357 phospholipid fatty acid abundance and C_{micr}. Nine 45 μm nylon mesh bags (4 × 5 cm) filled
358 with sand, which excluded roots but allowed access of fungi[45], were buried in November
359 2014 in each experimental plot and three bags were subsequently collected every four months
360 for one year. Phospholipid-derived fatty acids (PLFA), a proxy for total microbial biomass
361 abundance, were quantified in sand bags and native field soil following the protocol by Ref
362 46. $\delta^{13}C$ values of ground subsamples of this sand, native soil carbon, and aboveground plant
363 tissue (leaves of Eucalypts in April 2014) were used to estimate the fraction of the
364 accumulated carbon in sand bags that was derived from plant carbon using isotopic mass
365 balance. Due to the exclusion of roots, plant-derived carbon in bags can be attributed to
366 mycorrhiza. This plant-derived unitless fraction was then multiplied by the total
367 concentration of PLFA in sand bags to obtain the amount of the total PLFA contributed by
368 mycorrhiza (μg PLFA / g sand). To scale this to native soil PLFA concentrations we then
369 calculated the ratio between mycorrhizal PLFA in sand bags to total PLFA in soil

370 (representing the total microbial pool). Subsequently, to estimate C_{myco}, this ratio was
371 multiplied by the C_{micr} in each plot (Figure S7b).
372
373 **Leaflitter carbon pool (C_{lit})** was estimated based on leaf litter decomposition rate and leaf
374 litterfall data collected by litter baskets (Figure S8)[24]. Leaf litter decomposition rates were
375 estimated over 24 months using litter bags. Briefly, 2 g air-dried *Eucalyptus* litter was added
376 to 10 × 15 cm litter bags with a 2-mm mesh size. Twelve litter bags were randomly allocated
377 to 4 subplots within each treatment plot, and two litter bags were collected at 3, 6, 9, 12, 18
378 and 24 months to calculate mass loss over time (mass loss was averaged across the two
379 replicates from each subplot). A leaflitter exponential decay function was estimated for each
380 plot, based on data collected over this 24-month period. Leaf litterfall was estimated from
381 monthly collections of material from circular fine-mesh traps (each 0.2 m^2) at eight random
382 locations for each plot. We then applied the exponential decay function with litterfall biomass
383 to obtain C_{lit}, assuming a carbon fraction constant (Extended Data Table 2).
384
385 **Insect carbon pool (C_{ins})** was estimated based on two different sampling techniques, with
386 aerial insects partially estimated based on monthly dead insect data collected from circular
387 fine-mesh traps of 0.2 m^2 at eight random locations for each plot[47], and understory insects
388 estimated based on vacuum suction sampling from two locations for each plot[48]. The insect
389 biomass estimated based on these two sampling techniques may be a conservative estimate
390 (the frass produced would suggest presence of a larger insect biomass[49]); nevertheless, they
391 provided a direct estimate based on data collected *in situ*. The vacuum suction method
392 collected invertebrates from understorey vegetation in two 1 × 1 m subplots using a petrol-
393 powered 'G-Vac' vacuum device run on full-throttle for 20 s, for a total of five sampling
394 campaigns. Trapping locations were randomly chosen and fixed between sampling

campaigns. All invertebrates were sorted from debris, dried to constant weight at 60 °C and weighed on a microbalance with a precision of 1 μg. We assumed that vacuum samples as well as fine-mesh trap samples represent point estimates of invertebrate abundance. Then, the total biomass of sampled invertebrates was summed across sampling methods within each plot. A constant carbon fraction based on Ref 50 (Extended Data Table 2) was used to convert biomass into C_{ins} pool (Figure S9).

Ecosystem carbon uptake fluxes

Overstorey gross primary production (GPP_O) for each plot was provided by a stand-level model simulation (MAESPA), forced by hourly meteorological data, daily plot-specific leaf area index and leaf-scale treatment-specific photosynthetic parameters measured at the site (Figure S10a)[7,21]. In short, MAESPA was used as a tool to up-scale leaf-level gas exchange measurements to the whole canopy. In MAESPA, each plot consists of individual tree crowns that are located and parameterized with measured coordinates, crown size, and LAI. Each crown is divided into six layers, with leaf area uniformly distributed in each layer. Within each layer, the model simulates twelve grid points. The incident radiation on the sunlit and shaded leaf area at each grid point is calculated considering shading from upper crown and surrounding trees, solar angle (zenith and azimuth), and light source (diffuse or direct). Incident radiation is then used to calculate gas exchange using a Farquhar[51] formulation for photosynthesis and a Medlyn formulation[52] for stomatal conductance. The model was parameterized with treatment-specific leaf gas exchange measurements made *in situ*[7,53]. Leaf respiration and its temperature dependence were also quantified using data collected on site, then up-scaled to the canopy using MAESPA. The performance of the model was evaluated by comparing the simulated transpiration flux to sap flow data[54].

Similarly, **understorey GPP (GPP_u)** (Figure S10b) was simulated using MAESPA with photosynthetic parameters taken for the dominant grass *Microlaena stipoides*[41]. The parameterization of understory vegetation is different from that of the canopy. In each plot, the understory was assumed to form a single crown covering the whole plot (i.e., a circle with 12.5 m radius) at a height of 1.5 m. The LAI of the understory was estimated using phenology camera digital photographs taken at four permanent understorey vegetation monitoring subplots in each plot[43]. The average green pixel content was calculated from three photos in each subplot, and assumed to be the same as the fraction of absorbed PAR. We then assumed a light extinction coefficient of 0.5 in Beers' Law and calculated understorey LAI. Before 2014 there were 3 campaigns per year while from 2014 the cameras were automated, and we used the fortnightly averages. Leaf gas exchange parameters were obtained from Ref 41 and covered four to six campaigns per year from 2013 to 2016. We estimated a one-time g_1 parameter[52] for all plots and time, and assumed constant carboxylation rate (V_{cmax}) and electron transport rate (J_{max}) values at 25 ºC across plots. Basal leaf respiration rate and the temperature dependence of photosynthesis and respiration were assumed to be the same as those for the canopy. The understory simulation was conducted separately from the canopy, with canopy LAI from Ref 24 included to account for the shading from the canopy, branches and stems on the understory.

For the **methane net flux (CH_4),** air samples were collected following the closed-chamber method (or Non-Flow-Through Non-Steady-State [NFT-NSS] method). Seven replicated chambers were available for each plot. Headspace samples were collected monthly, over a period of one hour and analyzed by gas chromatography. Fluxes were estimated by a mixture of linear and quadratic regressions (depending on goodness-of-fit), assuming a constant air pressure of one atmosphere and correcting the air temperature inside the chambers for each

444 air sample[55]. The CH_4 fluxes are net fluxes, which represent the sum of: 1) CH_4 efflux
445 (emissions from the soil into the atmosphere); 2) CH_4 influx (uptake from the atmosphere
446 into soil). Here, the annual net CH_4 flux was an ecosystem influx and was presented as
447 positive values (Figure S11a).
448

449 *Production fluxes*

450 Plant **net primary production (NPP)** is the sum of overstorey leaf (NPP_{ol}), stem (NPP_{stem}),
451 fine root (NPP_{froot}), intermediate root (NPP_{iroot}), coarse root (NPP_{croot}), other (including twigs,
452 barks, and seeds; NPP_{other}), understorey aboveground (NPP_{ua}), and consumption of overstorey
453 leaf by insect herbivores (NPP_{ins}). NPP_{ol} and NPP_{other} were estimated based on monthly litter
454 data collected from circular fine-mesh traps of 0.2 m^2 at eight random locations for each plot
455 (Figure S12). Litter was sorted into leaf, twigs, bark, and seeds, dried to constant mass at
456 40 °C and weighed. A subsample was reweighed when dried to constant mass at 70 °C and a
457 small moisture correction[7] was applied to the leaf component of the whole dataset. NPP_{ol} was
458 computed as the sum of annual leaf litter, which excluded leaf consumption by insects. For
459 twigs, we assumed strictly annual turnover across the years. NPP_{stem} (Figure S13) and
460 NPP_{croot} (Figure S14) were estimated based on annual incremental change of stem biomass
461 and coarse root biomass, respectively. NPP_{froot} was estimated based on samples collected
462 from in-growth cores at four different locations per plot (Figure S14). NPP_{iroot} was estimated
463 based on a global mean coarse root turnover rate (0.3605 yr^{-1}) for evergreen broadleaf
464 forests[56], and the C_{iroot} pool in our dataset (Figure S14).
465

466 NPP_{ua} was estimated based on biomass clippings taken between 2015 - 2017, assuming one
467 understorey turnover per harvest interval (Figure S15). We used a clip-strip method of
468 biomass harvest as has been applied previously at the BioCON experiment[57]. Specifically,

four narrow strips, each with a size of 1 m × 0.1 m, were situated in each of the experimental plots at least 2 m away from the vertical pipes for FACE, while avoiding the understory shrubs. The understory herbaceous species were clipped approximately 1 cm above soil level. The total mass per harvest represents the total production. Biomass samples were oven dried for two days at 60 ^{o}C, and converted into carbon mass by applying a constant fraction (Extended Data Table 2).

NPP lost to overstorey leaf consumption by insect herbivores (NPP_{ins}) was estimated based on insect frass data (Frass) collected from the circular fine-mesh traps, and a relationship between frass mass and insect-consumed leaf mass derived based on multiple *Eucalyptus* tree species at different CO_2 concentrations (Figure S16a)[58,59]. Frass was estimated based on annual collection of frass biomass collected from the circular fine-mesh litter traps with their associated carbon content (Extended Data Table 2; Figure S16c).

Outfluxes

Leaching lost as **dissolved organic carbon (DOC)** from soils was estimated based on concentrations of DOC in soil solutions, provided by water suction lysimeter measurements[28]. Lysimeters were installed to two depths (0 - 15 cm and 35 - 75 cm, which is immediately above the impermeable layer). Here we assumed that DOC reaching deeper depth is lost from the system at a rate of 20 ml m^{-2} d^{-1}, which is an estimate of the daily drainage rate at the site (Figure S11b).

Plant autotrophic respiration (R_a) consists of overstorey leaf (R_{ol}), stem (R_{stem}), root (R_{root}), understorey aboveground (R_{ua}) (Figure S17), and growth respiration (R_{grow}) (Figure S18). R_{ol}

493 and R_{ua} were based on MAESPA simulation (Figure S17a, c), as described in the respective
494 GPP sections. R_{grow} was estimated by taking a constant fraction of 30% of total NPP as
495 measured directly on *E. tereticornis* trees[60].
496
497 R_{stem} was estimated from measurements of stem CO_2 efflux performed in three dominant
498 trees per plot (Figure S17b). Collars were horizontally attached to the stem at an approximate
499 height of 0.75 m, and R_{stem} (nmol CO_2 m^{-2} s^{-1}) was measured with a portable infrared gas
500 analyzer coupled to a soil respiration chamber adapted for this purpose[61]. Measurement
501 campaigns were performed every one or two months from December 2017 to October 2018,
502 and the relationship between R_{stem} and air temperature (T_{air}) was used to extrapolate R_{stem}
503 across the surveyed period, following $R_{stem} = 0.1866 \times 2.84^{Tair/10}$ ($r^2 = 0.42$, $p < 0.0001$). R_{stem}
504 was then upscaled to the stand level considering the ratio of stem axial surface per unit of soil
505 surface measured per plot. Stem surface area was inferred from the measured tree diameter
506 based on dendrometer, and a relationship between diameter and stem surface area estimated
507 from the Terrestrial Laser Scanning (TLS) data. Stem surface area and diameter in the TLS
508 data was estimated through quantitative structure models presented in Ref. 62 and 63. TLS
509 data were acquired with a RIEGL VC-400 terrestrial laser scanner (RIEGL Laser
510 Measurement Systems GmbH). Stem surface area was derived from the TLS data following a
511 two-step approach: (i) manually extracting single trees from the registered TLS point cloud;
512 and (ii) deriving parameters for an extracted single tree. Once a tree is extracted from the
513 point cloud, the next step was to strip off the leaves, and segment the point cloud into stem
514 and branches. Finally, the surface of the segments was reconstructed with geometric
515 primitives (cylinders). The method used a cover set approach, where the point cloud was
516 partitioned into small subsets, which correspond to small connected patches in the tree
517 surface.

R_{root} was partitioned into fine root (R_{froot}), intermediate root (R_{iroot}), and coarse root (R_{croot}) respiration (Figure S17d). Mass-based rates of fine root and intermediate root respiration (nmol CO_2 DM g^{-1} s^{-1}) were measured for detached roots sampled by soil cores at 10 cm soil depth at four subplots per plot with a portable infrared gas analyzer coupled to a small root chamber. Measurement campaigns were performed every one or two months from November 2018 to July 2019. The relationship between root respiration and soil temperature (T_{soil}) at 10 cm soil depth was used to extrapolate the corresponding root respiration rates across the surveyed period, following the equations: $R_{froot} = 1.138 \times 1.614^{0.0479 \times Tsoil}$ ($r^2 = 0.36$, $p < 0.0001$, RMSE = 1.054), and $R_{iroot} = 0.9764 \times 1.586^{0.0641 \times Tsoil}$ ($r^2 = 0.52$, $p < 0.0001$, RMSE = 0.597). The mass-based rate of coarse root respiration was assumed to be the same as the mass-based rate of stem respiration. R_{froot}, R_{iroot} and R_{croot} were then upscaled to the stand level to obtain R_{root} with fine root, intermediate root, and coarse root biomass, respectively.

Carbon efflux due to insect respiration (R_{ins}) was estimated as the net difference between NPP_{ins} and Frass, assuming no net change in insect biomass (Figure S16b).

Soil respiration (R_{soil}): The rate of soil CO_2 efflux was measured at eight locations within each plot, where a permanent PVC collar inserted into the soil was co-located with soil TDR probes for continuous measurements of soil temperature (5-cm-depth) and volumetric water content (0 to 21-cm-depth; CS650-L; Campbell Scientific, Logan, UT, USA). R_{soil} was measured manually at all collar locations every 2-3 weeks, in addition to 30-minute measurements using automated chambers (Li-8100-103; Licor) at one location within each plot, resulting in >300,000 observations over the study period[26]. These data were used to parameterize a semi-mechanistic model of R_{soil}, in which R_{soil} was predicted based on

543 measurements of soil properties, soil physics, and measured soil temperature and volumetric
544 water content[64]. This model successfully recreated the observed fluxes (r^2 between predicted
545 and observed survey R_{soil} was 0.65)[26]. Annual sums of R_{soil} were derived by summing the
546 averaged daily fluxes over eight locations within each plot, where daily fluxes at each
547 location were predicted based on the semi-mechanistic model and daily soil temperature and
548 volumetric water content data taken adjacent to each measurement collar. Soil heterotrophic
549 respiration (R_{hetero}) was taken as the net difference between R_{soil} and R_{root} (Figure S19). Total
550 ecosystem respiration (R) was calculated as the sum of R_a, R_{hetero}, R_{ins}, and VC.
551
552 **Volatile carbon (VC;** Figure S20**)** flux as isoprene (C_5H_8) and monoterpenes was estimated
553 using the Model of Emissions of Gases and Aerosols from Nature (MEGAN)[65]. Isoprene
554 represents over half of all volatile organic carbon species emitted by vegetation globally, and
555 is the dominant source of VC emission at our site. A MEGAN box-model was built from the
556 version used in Ref. 66, centered on the EucFACE facility to calculate hourly emissions of
557 isoprene across the period 2013-2016 for all six plots:
558 $$VC = EF \times LAI \times \gamma$$
559 Where EF is the compound-specific basal emission factor, γ is the emission activity factor,
560 accounting for changes in the emission response due to light, temperature, leaf age and soil
561 moisture. The MEGAN simulations were driven by daily input data of LAI, soil moisture,
562 and hourly input data of photosynthetic active radiation, temperature, atmospheric pressure,
563 wind speed and relative humidity.
564
565 The isoprene EFs for ambient and elevated CO_2 plots were derived from in-line
566 photosynthetic gas-exchange measurements coupled with simultaneous volatile isoprenoid
567 sampling. The isoprene was collected onto sterile stainless steel thermal desorption tubes at

568 the same time as gas exchange was measured, and these were capped and later thermally
569 desorbed for off-line volatile analysis in the laboratory using a Shimadzu 2010 Plus GC-MS
570 system connected to a Shimadzu TD20 automated cartridge desorber. The sampling and GC-
571 MS analysis methodology is described in detail in Ref 67. The chromatographic peaks were
572 identified by comparing them to an isoprene standard and reference mass spectra in the NIST
573 Mass Spectral Library (https://www.nist.gov/srd). Monoterpene emissions were sampled
574 during February 2018 using a push-pull headspace technique[68] from enclosed branches
575 containing approximately 10 leaves and trapped on adsorbent cartridges (150 mg Tenax TA
576 and 200 mg Carbograph 1TD, Markets International Limited, United Kingdom) at an outflow
577 rate of 200 ml min^{-1} for 15 min. Before each measurement, the sampling system was
578 equilibrated for 15 min at an inflow rate of 1000 mol min^{-1}. Monoterpenes were analyzed by
579 gas chromatography-mass spectrometry (R7890A Series GC coupled with a 5975C inert
580 MSD/DS Performance Turbo EI System, Agilent Technologies, Inc., Santa Clara, CA, USA),
581 as described by Ref 69. The obtained chromatograms were deconvoluted, analyzed and data
582 retrieved using the software PARADISe[70] version 3.88. Identification of compounds was
583 performed using analytical standards and according to their mass spectra in the NIST11
584 library. Pure analytical standards were used for quantification. The box-model produced
585 isoprene and monoterpenes were converted to carbon content using the respective molecular
586 mass ratios.
587
588 *Net Ecosystem Production*
589 Net ecosystem production (NEP) was estimated based on three different methods that
590 estimated NEP in relatively independent ways (Figure 3), similar to Ref 71. The first method
591 considered NEP as the difference between total ecosystem influx and total ecosystem outflux
592 (i.e. In - Out), which relied on both process-based modeling and empirical upscaling of

593 respiratory fluxes collected from the field. The second method considered NEP as NPP minus
594 R_{hetero} (i.e. NPP - R_{hetero}), with NPP relying mostly on litter-based production estimates, and
595 R_{hetero} relying on R_{soil} and R_{root} estimates. The third method considers NEP as the sum of
596 changes in carbon pools over time in the ecosystem (i.e. ΔC_{pools}), which was mostly
597 determined by biomass estimates. Equations for each method are provided below:

Method	**NEP =**
In - Out	$GPP_o + GPP_u + CH_4 - R_{ol} - R_{stem} - R_{soil} - R_{ua} - R_{ins} - DOC - VC - R_{grow}$
NPP - R_{hetero}	$NPP_{ol} + NPP_{stem} + NPP_{froot} + NPP_{iroot} + NPP_{croot} + NPP_{other} + NPP_{ua} + NPP_{ins} - R_{hetero}$
ΔC_{pools}	$\Delta C_{soil}+\Delta C_{ol}+\Delta C_{stem}+\Delta C_{croot}+\Delta C_{froot}+\Delta C_{iroot}+\Delta C_{ua}+\Delta C_{lit}+\Delta C_{ins}+\Delta C_{micr}+\Delta C_{myco}$

598

599 **Carbon budget evaluation**

600 We evaluated the mass balance of our estimated ecosystem carbon budget in two ways.
601 Firstly, we compared model simulated GPP with the aggregated sum of NPP and R_a
602 (Extended Data Figure 3a, b). GPP was simulated by a stand-level ecophysiological model,
603 driven by hourly meteorological data and parameterized with site-specific ecological data[20].
604 This GPP should equal to the aggregation of NPP ($NPP_{ol} + NPP_{stem} + NPP_{froot} + NPP_{iroot} +$
605 $NPP_{croot} + NPP_{other} + NPP_{ua} + NPP_{ins}$) and R_a fluxes ($R_{ol} + R_{stem} + R_{root} + R_{ua} + R_{grow}$), which
606 were mostly extrapolated based on field data. Secondly, R_{soil} estimated based on soil collar
607 flux measurements[24] was evaluated against the sum of litterfall and R_{root} (Extended Data
608 Figure 3c, d), assuming minimal changes in soil carbon stock (as change over this short
609 period of time is beyond the detection limit in a complex and slow-growing mature forest
610 ecosystem like EucFACE). Here, litterfall was the sum of $NPP_{ol} + NPP_{froot} + NPP_{iroot} +$

611 NPP_{other} + NPP_{ua} + Frass, and R_{root} was extrapolated based on root biomass and temperature
612 functions.
613
614 **Statistical analyses**
615 We performed linear mixed-model analysis using the "lmer" function within the "lme4"
616 package[72] in software R[73] to determine the CO_2 treatment effect on all reported variables. All
617 fluxes were reported at an annual rate (g C m^{-2} yr^{-1}). In our model, date and CO_2 treatment
618 were considered as fixed factors, plot as a random factor, and plot-specific pre-treatment LAI
619 (i.e. 4-month average LAI before full CO_2 treatment was switched on) as a covariate to
620 account for pre-treatment differences among treatment plots. Normalizing all response
621 variables with a covariate that integrates light, water and nutrient constraints helps to isolate
622 the CO_2 effect[23], as has been done previously at the site[24] and elsewhere[8,23]. Confidence
623 intervals for the CO_2 effect size of individual variables were reported using the function
624 "confint", which applies quantile functions for the t-distribution after model fitting.
625 Confidence intervals for the predicted flux and pool were reported as the standard deviation
626 of the plot-specific totals (n = 3). Similarly, confidence intervals for the aggregated fluxes
627 (e.g. NPP) were reported by summing individual component fluxes that constitutes the
628 aggregated flux for each plot and computing the standard deviations across plots (n = 3).
629 Finally, confidence intervals for the CO_2 effect size (SD_{agg}) of some aggregated fluxes (e.g.
630 NPP) were calculated by pooling the standard deviations of the aggregated fluxes for ambient
631 (SD_{amb}) and elevated CO_2 treatment (SD_{ele}), following:

$$SD_{agg} = \sqrt{\frac{SD_{amb}^2 + SD_{ele}^2}{2}}$$

632

Uncertainty analysis

We applied a Markov Chain Monte Carlo (MCMC) data assimilation algorithm to a simplified carbon cycle framework to make inference of the uncertainties around the fate of carbon in our carbon budget. We simplified our carbon budget into eight pools (Extended Data Figure 7), namely, leaf (C'_{leaf}, which includes overstorey and understorey), wood (C'_{wood}, which includes stem and coarse root), root (C'_{root}, which includes fine root and intermediate root), aboveground litter (C'_{aglit}), belowground litter (C'_{bglit}), mycorrhizae (C'_{myco}), microbe (C'_{micr}), and soil (C'_{soil}). Here, C'_{aglit} and C'_{bglit} were assumed unknowns and inferred from the analysis. Net primary production (NPP) was calculated as the difference of gross primary production (GPP) and autotrophic respiration (R_a). NPP was then allocated into the four plant carbon pools (C'_{leaf}, C'_{wood}, C'_{root}, and C'_{myco}), with the respective fitted allocation coefficients (a_{leaf}, a_{wood}, a_{root}, and a_{myco}) being inferred. It has been shown that plant carbon allocation to mycorrhizal fungi may be an important flux in forest carbon budget calculation[74]. Turnover rates of C'_{leaf}, C'_{root}, C'_{myco}, C'_{aglit}, C'_{bglit}, C'_{micr} and C'_{soil} were represented by the corresponding turnover coefficients (τ_{leaf}, τ_{wood}, τ_{root}, τ_{myco}, τ_{aglit}, τ_{bglit}, τ_{micr}, τ_{soil}), all of which were assumed unknowns except τ_{wood} (estimated based on litter basket data of twigs, barks and seeds) and τ_{aglit} (estimated from the leaf litter decomposition data). For carbon leaving from C'_{aglit}, C'_{bglit} and C'_{micr}, we inferred the corresponding fractional coefficient that determines the fraction of carbon entering into the next pool (f'_{aglit}, f'_{bglit}, and f'_{micr}), and assumed the remainder to be respired as part of R_{hetero}. The turnover of soil carbon (i.e. τ_{soil}) also contributed to R_{hetero}. In total, we fitted 2 pools, 4 allocation coefficients, 6 turnover rates, and 3 fractional coefficients using the MCMC algorithm.

We used plot-level estimates of GPP, R_a, R_{hetero}, carbon pools and changes in pools to constrain the MCMC fitting. We assumed uniform parameter distributions and a burn-in

658 coefficient of 10%. Chain lengths were set at 200,000 for the ambient CO_2 plots and 500,000
659 for the elevated plots. The longer chain length for the elevated plots was due to the smaller
660 proposal step size for these plots to meet an acceptance rate of around 20%. We reported the
661 means and standard deviation of the estimated parameters at the treatment level in Extended
662 Data Figure 7.
663

664 **Data statement**

665 Data will be available via Figshare (DOI: 10.6084/m9.figshare.11634315) with the
666 publication of the manuscript. Code to process the data is available via GitHub
667 (https://github.com/mingkaijiang/EucFACE_Carbon_Budget/releases/tag/V20200120).

668 **References for main text**

669 1. Le Quéré, C.L. *et al*. Global carbon budget 2018. *Earth Syst. Sci. Data* **10**, 2141-2194
670 (2018).
671 2. Schimel, D., Stephens, B.B., and Fisher, J.B. Effect of increasing CO_2 on the
672 terrestrial carbon cycle. *Proc. Natl. Acad. Sci. USA* **112**, 436-441 (2015).
673 3. Walker, A.P. *et al*. Decadal biomass increment in early secondary successional woody
674 ecosystems is increased by CO_2 enrichment. *Nat. Commun.* **10**, 454,
675 https://doi.org/10.1038/s41467-019-08348-1 (2019).
676 4. Norby, R.J. and Zak, D.R. Ecological lessons from Free-Air CO_2 Enrichment (FACE)
677 experiments. *Annu. Rev. Ecol. Evol. Syst.* **42**, 181-203 (2011).
678 5. Leuzinger, S. and Hattenschwiler, S. Beyond global change: lessons from 25 years of
679 CO_2 research. *Oecologia* **171**, 639-651 (2013).
680 6. Arora, V.K. *et al.* Carbon-concentration and carbon-climate feedbacks in CMIP5
681 Earth system models. *J. Clim.* **26**, 5289-5214 (2013).
682 7. Ellsworth, D.S. *et al.* Elevated CO_2 does not increase eucalypt forest productivity on a
683 low-phosphorus soil. *Nat. Clim. Change* **7**, 279-282 (2017).
684 8. Körner, C. *et al.* Carbon flux and growth in mature deciduous forest trees exposed to
685 elevated CO_2. *Science* **309**, 1360-1362 (2005).
686 9. Ryan, M.G. Three decades of research at Flakaliden advancing whole-tree physiology,
687 forest ecosystem and global change research. *Tree Physiol*. **33**, 1123-1131 (2013).
688 10. Klein, T. *et al.* Growth and carbon relations of mature *Picea abies* trees under 5 years
689 of free-air CO_2 enrichment. *J. Ecol.* **104**, 1720-1733 (2016).
690 11. Norby, R.J. *et al.* Model-data synthesis for the next generation of forest free-air CO_2
691 enrichment (FACE) experiments. *New Phytol.* **209**, 17-28 (2016).

12. Pugh, T.A.M. *et al.* Role of forest regrowth in global carbon sink dynamics. *Proc. Natl. Acad. Sci. USA* **116**, 4382-4387 (2019).
13. Grassi, G. *et al.* The key role of forests in meeting climate targets requires science for credible mitigation. *Nat. Clim. Change* **7**, 220-226 (2017).
14. Peñuelas, J. *et al.* Shifting from a fertilization-dominated to a warming-dominated period. *Nat. Ecol. Evol.* **1**, 1438-1445 (2017).
15. Luo, Y. *et al.* Progressive nitrogen limitation of ecosystem response to rising atmospheric carbon dioxide. *BioScience* **54**, 731-739.
16. DeLucia, E.H. *et al.* Net primary production of a forest ecosystem with experimental CO_2 enrichment. *Science* **285**, 1177-1179 (1999).
17. Crous, K., Ósvaldsson, A., and Ellsworth, D.S. Is phosphorus limiting in a mature *Eucalyptus* woodland? Phosphorus fertilization stimulates stem growth. *Plant Soil* **391**, 293-305 (2015).
18. Medlyn, B.E. *et al.* Using models to guide field experiments: a priori predictions for the CO_2 response of a nutrient- and water-limited native Eucalypt woodland. *Global Change Biol.* **22**, 2834-2851 (2016).
19. Medlyn, B.E. *et al.* Using ecosystem experiments to improve vegetation models. *Nat. Clim. Change* **5**, 528-534 (2015).
20. Friedlingstein, P. *et al*. Uncertainties in CMIP5 climate projections due to carbon cycle feedbacks. *J. Clim.* **27**, 511-526 (2014).
21. Yang, J. *et al.* Low sensitivity of gross primary production to elevated CO_2 in a mature Eucalypt woodland. *Biogeosciences*. DOI: https://doi.org/10.5194/bg-2019-272 (2020).

715 22. De Lucia, E.H., Drake, J.E., Thomas, R.B., and Gonzalez-Meler, M. Forest carbon
716 use efficiency: is respiration a constant fraction of gross primary production? *Global*
717 *Change Biol.* **13**, 1157-1167 (2007).
718 23. Norby, R.J. Forest canopy productivity index. *Nature* **381**, 564 (1996).
719 24. Duursma, R.A. *et al*. Canopy leaf area of a mature evergreen Eucalyptus woodland
720 does not respond to elevated atmospheric CO_2 but tracks water availability. *Global*
721 *Change Biol*. **22**, 1666-1676 (2016).
722 25. Drake, J.E. *et al.* Short-term carbon cycling responses of a mature eucalypt woodland
723 to gradual stepwise enrichment of atmospheric CO_2 concentration. *Global Change*
724 *Biol.* **22**, 380-390 (2016).
725 26. Drake, J.E. *et al.* Three years of soil respiration in a mature eucalypt woodland
726 exposed to atmospheric CO_2 enrichment. *Biogeochemistry* **139**, 85-101 (2018).
727 27. Drake, J.E. *et al.* Increases in the flux of carbon belowground stimulate nitrogen
728 uptake and sustain the long-term enhancement of forest productivity under elevated
729 CO_2. *Ecol. Lett*. **14**, 349-357 (2011).
730 28. Hasegawa, S., Macdonald, C.A., and Power, S.A. Elevated carbon dioxide increases
731 soil nitrogen and phosphorus availability in a phosphorus-limited *Eucalyptus*
732 woodland. *Global Change Biol.* **22**, 1628-1643 (2016).
733 29. Ochoa-Hueso, R. *et al.* Rhizosphere-driven increase in nitrogen and phosphorus
734 availability under elevated atmospheric CO_2 in a mature *Eucalyptus* woodland. *Plant*
735 *Soil* **416**, 283-295 (2017).
736 30. Crous, K.Y., Wujeska-Klause, A., Jiang, M., Medlyn, B.E. and Ellsworth, D.S.
737 Nitrogen and phosphorus retranslocation of leaves and stemwood in a mature
738 *Eucalyptus* forest exposed to 5 years of elevated CO_2. *Front. Plant Sci.* **10**:664, doi:
739 10.3389/fpls.2019.00664 (2019).

31. Zaehle, S. *et al*. Evaluation of 11 terrestrial carbon-nitrogen cycle models against observations from two temperature Free-Air CO_2 Enrichment studies. *New Phytol.* **202**, 803-822 (2014).
32. Fleischer, K. *et al.* Amazon forest response to CO_2 fertilization dependent on plant phosphorus acquisition. *Nat. Geosci.* **12**, 736-741 (2019).
33. Todd-Brown, K.E.O. *et al*. Changes in soil organic carbon storage predicted by earth system models during the 21st century. *Biogeosciences*, **11**, 2341-2356 (2014).
34. Kuzyakov, Y., Horwath, W.R., Dorodnikov, M. and Blagodatskaya, E. Review and synthesis of the effects of elevated atmospheric CO_2 on soil processes: no changes in pools, but increased fluxes and accelerated cycles. *Soil Biol. Biochem*. **128**, 66-78 (2019).
35. Luyssaert, S. *et al.* Old-growth forests as global carbon sinks. *Nature* **455**, 213-215 (2008).
36. Jones, C. *et al*. 21st century compatible CO_2 emissions and airborne fraction simulated by CMIP5 Earth System models under 4 representative concentration pathways. *J. Clim.* **26**, doi:10.1175–JCLI–D–12–00554.1 (2013).

Reference for Methods

37. Australia Government Department of Agriculture, Fisheries and Forestry. Australia's agriculture, fisheries and forestry at a glance 2012. Canberra, Australia (2012).
38. Food and Agricultural Organization of the United Nations. Global Forest Resources Assessment 2000. FAO Forestry Paper 140. Rome, Italy (2001).

763 39. Gimeno, T.E., McVicar, T.R., O'Grady, A.P., Tissue, D.T. and Ellsworth, D.S.
764 Elevated CO_2 did not affect the hydrological balance of a mature native *Eucalyptus*
765 woodland. *Global Change Biol.* **24**, 3010-3024 (2018).
766 40. Hasegawa, S. *et al*. Elevated CO_2 concentrations reduce C_4 cover and decrease
767 diversity of understorey plant community in a *Eucalyptus* woodland. *J. Ecol.* **106**,
768 1483–1494 (2018).
769 41. Pathare, V.S. *et al*. Water availability affects seasonal CO_2-induced photosynthetic
770 enhancement in herbaceous species in a periodically dry woodland. *Global Change*
771 *Biol*. **23**, 5164–5178 (2017).
772 42. Paul, K.I. *et al.* Development and testing of allometric equations for estimating above-
773 ground biomass of mixed-species environmental plantings. *For. Ecol. Manage.* **310**,
774 483-494 (2013).
775 43. Collins, L. *et al.* Understorey productivity in temperate grassy woodland responds to
776 soil water availability but not to elevated CO_2. *Global Change Biol*. **24**, 2366-2376
777 (2018).
778 44. Snowdon, P. *et al.* National carbon accounting system technical report no. 17.
779 Australian Greenhouse Office, Canberra, Australia (2000).
780 45. Wallander, H. *et al.* Evaluation of methods to estimate production, biomass and
781 turnover of ectomycorrhizal mycelium in forests soils – A review. *Soil Biol. Biochem.*
782 **57**, 1034–1047 (2013).
783 46. Buyer, J.S. and Sasser, M. High throughput phospholipid fatty acid analysis of soils.
784 *Appl. Soil Ecol*. **61**, 127–130 (2012).
785 47. Gherlenda, A.N., Esveld, J.L., Hall, A.A.G., Duursma, R.A. and Riegler, M. Boom
786 and bust: rapid feedback responses between insect outbreak dynamics and canopy leaf
787 area impacted by rainfall and CO_2. *Global Change Biol*. **22**, 3632-3641 (2016).

48. Facey, S.L. *et al*. Atmospheric change causes declines in woodland arthropods and impacts specific trophic groups. *Agr. Forest Entomol.* **19**, 101-112 (2017).

49. Murray, T.J., Tissue, D.T., Ellsworth, D.S. and Riegler, M. Interactive effects of pre-industrial, current and future CO_2 and temperature on an insect herbivore of *Eucalyptus*. *Oecologia* **171**, 1025-1035 (2013).

50. Trakimas, G. *et al*. Ecological Stoichiometry: a link between developmental speed and physiological stress in an omnivorous insect. *Front. Behav. Neurosci*. **13**:42, https://doi.org/10.3389/fnbeh.2019.00042 (2019).

51. Farquhar, G.D. von Caemmerer, S. and Berry, J.A. A biochemical model of photosynthetic CO_2 assimilation in leaves of C3 species. *Planta* **149**, 78–90 (1980).

52. Medlyn, B.E. *et al.* Reconciling the optimal and empirical approaches to modelling stomatal conductance. *Global Change Biol*. **17**, 2134–2144 (2011).

53. Gimeno, T.E. *et al*. Conserved stomatal behavior under elevated CO_2 and varying water availability in a mature woodland. *Funct. Ecol*. **30**, 700-709 (2016).

54. Yang, J. *et al.* Incorporating non-stomatal limitation improves the performance of leaf and canopy models at high vapor pressure deficit. *Tree Physiol*. DOI: https://doi.org/10.1093/treephys/tpz103 (2019).

55. Martins, C.S.C. *et al.* Identifying environmental drivers of greenhouse gas emissions under warming and reduced rainfall in boreal-temperate forests. *Funct. Ecol.* **31**, 2356–2368 (2017).

56. Zhang, X. and Wang, W. The decomposition of fine and coarse roots: their global patterns and controlling factors. *Sci. Rep.* **5**:09940 (2015).

57. Reich, P.B. *et al.* Plant diversity enhances ecosystem responses to elevated CO_2 and nitrogen deposition. *Nature* **410**, 809-810 (2001).

812 58. Gherlenda, A.N., Moore, B.D., Haigh, A.M., Johnson, S.N. and Riegler, M. Insect
813 herbivory in a mature *Eucalyptus* woodland canopy depends on leaf phenology but
814 not CO_2 enrichment. *BMC Ecol.* **16**, 47 (2016).
815 59. Gherlenda, A.N. *et al*. Precipitation, not CO_2 enrichment, drives insect herbivore frass
816 deposition and subsequent nutrient dynamics in a mature *Eucalyptus* woodland. *Plant*
817 *Soil* **399**, 29-39 (2016).
818 60. Drake, J.E. *et al*. The partitioning of gross primary production for young *Eucalyptus*
819 *tereticornis* trees under experimental warming and altered water availability. *New*
820 *Phytol*. **222**, 1298-1312 (2019).
821 61. Salomón, R.L., Steppe, K., Crous, K.Y., Noh, N.J. and Ellsworth, D.S. Elevated CO_2
822 does not affect stem CO_2 efflux nor stem respiration in dry *Eucalyptus* woodland, but
823 it shifts the vertical gradient in xylem CO_2. *Plant Cell Environ.* **42**, 2151-2164 (2019).
824 62. Raumonen, P. *et al.* Fast Automatic Precision Tree Models from Terrestrial Laser
825 Scanner Data. *Remote Sens.* **5**, 491-520 (2013).
826 63. Calders, K. *et al.* Nondestructive estimates of above-ground biomass using terrestrial
827 laser scanning. *Methods Ecol. Evol.* **6**, 198-208 (2015).
828 64. Davidson, E.A., Samanta, S., Caramori, S.S. and Savage, K. The Dual Arrhenius and
829 Michaelis–Menten kinetics model for decomposition of soil organic matter at hourly
830 to seasonal time scales. *Global Change Biol.* **18**, 371-384 (2012).
831 65. Guenther, A.B. *et al.* The Model of Emissions of Gases and Aerosols from Nature
832 version 2.1 (MEGAN2.1): an extended and updated framework for modeling biogenic
833 emissions. *GeoSci. Model Dev*. **5**, 1471-1492 (2012).
834 66. Emmerson, K.M., Palmer, P.I., Thatcher, M., Haverd, V. and Guenther, A.B.
835 Sensitivity of isoprene emissions to drought over south-eastern Australia: Integrating

models and satellite observations of soil moisture, *Atmos. Environ*. **209**, 112-124 (2019).

67. Kännaste, A., Copolovici, L. and Niinemets, Ü. Gas chromatography mass-spectrometry method for determination of biogenic volatile organic compounds emitted by plants. In: Plant isoprenoids: methods and protocols. Eds. M. Rodríguez-Concepción, Humana Press, New York. pp. 161-169 (2014).
68. Tholl, D. *et al*. Practical approaches to plant volatile analysis. *Plant J*. **45**, 540 – 560 (2006).
69. Li, T., Holst, T., Michelsen, A. and Rinnan, R. Amplification of plant volatile defense against insect herbivory in a warming Arctic tundra. *Nat. Plants* **5**, 568-475 (2019).
70. Johnsen, L.G., Skou, P.B., Khakimov, B., and Bro, R. Gas chromatography – mass spectrometry data processing made easy. *J. Chromatogr. A*. **1503**, 57-64 (2017).
71. Keith, H. *et al*. Multiple measurements constrain estimates of net carbon exchange by a *Eucalyptus* forest. *Agric. For. Meteorol.* **149**, 535-558 (2009).
72. Bates, D., Machler, M., Bolker, B.M., and Walker, S.C. Fitting linear mixed-effects models using lme4. *J. Stat. Softw*. **67**, 1-48 (2015).
73. R Core Team. R: A language and environment for statistical computing. R Foundation for Statistical Computing, Vienna, Austria. URL https://www.R-project.org/ (2018).
74. Ouimette, A.P. *et al.* Accounting for carbon flux to mycorrhizal fungi may resolve discrepancies in forest carbon budgets. *Ecosystems* https://doi.org/10.1007/s10021-019-00440-3 (2019).
75. Harrison, I., Jones, P.D., Osborn, T.J. and Lister, D.H. Updated high-resolution grids of monthly climatic observations – the CRU TS3.10 dataset. *Int. J. Climatol.* **34**, 623-642 (2014).

76. Olson, D.M. *et al*. Terrestrial ecoregions of the world: a new map of life on Earth. *BioScience* **51**, 933-938 (2001).

77. Jiang, M., Felzer, B.S., Nielsen, U.N. and Medlyn, B.E. Biome-specific climatic space defined by temperature and precipitation predictability. *Global Ecol. Biogeogr.* **26**, 1270-1282 (2017).

78. Scarascia-Mugnozza, G. *et al*. Response to elevated CO_2 of a short rotation, multispecies Poplar plantation: the POPFACE/EUROFACE experiment. In Managed Ecosystems and CO_2. Eds. Nösberger, J., *et al*. Berlin, Heidelberg, New York: Springer Verlag. pp 173–195 (2006).

79. Linden, S. NPP Boreal Forest: Flakaliden, Sweden, 1986-1996, R1. Data set. Available on-line [http://daac.ornl.gov] from Oak Ridge National Laboratory Distributed Active Archive Center, Oak Ridge, Tennessee, USA. DOI:10.3334/ORNLDAAC/201 (2013).

80. Anderson-Teixeira, K.J. *et al.* ForC: a global database of forest carbon stock and fluxes. *Ecology* **99**, 1507-1507 (2018).

81. Shangguan, W. Dai, Y., Duan, Q., Liu, B. and Yuan, H. A global soil data set for earth system modelling. *J. Adv. Model Earth Sys*. **6**, 249-263 (2014).

82. Yang, X., Post, W.M., Thornton, P.E. and Jain, A. Global gridded soil phosphorus distribution maps at 0.5-degree resolution. Data set. Available on-line [http://daac.ornl.gov] from Oak Ridge National Laboratory Distributed Active Archive Center, Oak Ridge, Tennessee, USA. http://dx.doi.org/10.3334/ORNLDAAC/1223 (2014).

Acknowledgements

EucFACE was built as an initiative of the Australian Government as part of the Nation-building Economic Stimulus Package, and is supported by the Australian Commonwealth in collaboration with Western Sydney University. We acknowledge the technical support by V. Kumar, C. McNamara and S. Wohl, and the team of people who have assisted with data collection. The *Eucalyptus* tree vector in Figure 1 is from Heydon, L. *Eucalyptus spp*. Integration and Application Network, University of Maryland Center for Environmental Science (ian.umces.edu/imagelibrary/). This work was partially supported by the following grants from the Australian Research Council (ARC): DP130102501 (to JRP and ICA), DP170104634 (to BKS and PBR), DP110105102 and DP160102452 (to DSE). MGDK acknowledges funding from the ARC Centre of Excellence for Climate Extremes (CE170100023), the ARC Discovery Grant (DP190101823) and support from the NSW Research Attraction and Acceleration Program. RLS received funding from Research Foundation Flanders and the European Union's Horizon 2020 research and innovation programme under the Marie Skłodowska Curie grant agreement no. 665501. RO-H. is financially supported by a Ramón y Cajal Fellowship from MICIU (RYC-2017-22032). EHJN and BMDS received funding from VILLUM Center for Plant Plasticity (VKR023054), VILLUM Young Investor Program fellowship (VKR013167), and a Danish Independent Research Council Sapere Aude Research Talent Post-Doctoral Stipend (6111-00379B). ÜN and AK have been supported by the European Commission through the European Regional Fund (Center of Excellence EcolChange).

Author contributions

MJ, BEM, RAD and JED designed the synthesis, compiled the data, and performed the analyses. MJ, BEM, JED, RAD, ICA, CVMB, MMB, YC, LC-G, LC, KYC, BMDS, SLF, ANG, TEG, SH, SNJ, AK, CAM, KM, BDM, LN, EHJN, UNN, ÜN, NJN, RO-H, VSP, EP, JP, JP, JRP, SAP, PBR, AAR, MR, RR, PR, RLS, BKS, BS, MGT, JKMW, AW-K, JY and DSE collected data and contributed to data analyses. MJ performed data assimilation analysis, with contributions from MGDK and BEM. JY and BEM performed the MAESPA model simulations, with contributions from MGDK and RAD. JED and AAR performed soil respiration gap-filling and modelling. KME performed the MEGAN model simulation. MJ and LC-G conceptualized Figure 1, and LC-G implemented the graphic design. MJ wrote the initial manuscript, with significant input from BEM, JED, BS, PBR, SZ, MGDK, MGT and DSE. All authors edited and approved the manuscript.

Competing financial interests

None declared.

Materials and Correspondence

Correspondence should be directed to MJ (m.jiang@westernsydney.edu.au) and BEM (b.medlyn@westernsydney.edu.au).

924 **Figure legend**

925

926 **Figure 1. A comprehensive carbon budget under ambient and elevated CO_2 treatment**
927 **in a mature forest ecosystem.** Diamond boxes are gross primary production for overstorey
928 (GPP_o) and understorey (GPP_u), respectively. Squared boxes are average carbon stocks over
929 the experimental period (C_{pools}, g C m^{-2}), including overstorey leaf (C_{ol}), stem (C_{stem}), coarse
930 root (C_{croot}), fine root (C_{froot}), intermediate root (C_{iroot}), understorey aboveground (C_{ua}), leaf
931 litter (C_{lit}), soil (C_{soil}), microbe (C_{micr}), aboveground insect (C_{ins}), and mycorrhizae (C_{myco}).
932 Unboxed variables are carbon fluxes (g C m^{-2} yr^{-1}), including net primary production of
933 overstorey leaf (NPP_{ol}), stem (NPP_{stem}), coarse root (NPP_{croot}), fine root (NPP_{froot}),
934 intermediate root (NPP_{iroot}), and understorey aboveground (NPP_{ua}), overstorey leaf
935 consumption by insects (NPP_{ins}), respiration fluxes of overstorey leaf (R_{ol}), stem (R_{stem}), root
936 (R_{root}), understorey aboveground (R_{ua}), growth (R_{grow}), insect (R_{ins}), heterotroph (R_{hetero}), and
937 soil (R_{soil}), and volatile carbon emission (VC), frass production (Frass), dissolved organic
938 carbon (DOC), and soil methane net uptake (CH_4). Solid arrow lines are fluxes entering a
939 pool, dotted arrow lines are fluxes leaving a pool. The changes in each carbon pool over time
940 ($\Delta C_{pools,}$ g C m^{-2} yr^{-1}) are reported in Extended Data Figure 6. Blue italic values are means ±
941 one standard deviation of the ambient CO_2 treatment (n=3), whereas red values are means ±
942 one standard deviation of the elevated CO_2 treatment (n=3). All values are normalized by a
943 linear mixed-model with plot-specific pre-treatment leaf area index as a covariate to account
944 for pre-existing differences. A summary of variable definitions and data availability is
945 provided in Extended Data Table 1.

Figure 2. The fate of additional carbon fixed under elevated CO_2 (eCO_2) in a mature forest ecosystem. a) Column "GPP" represents the total eCO_2-induced increases in overstorey and understorey gross primary production (GPP_o and GPP_u, respectively), "NPP + R_a" represents the sum of net primary production and autotrophic respiration response, "R + ΔC_{pools}" represents the sum of ecosystem respiration and change in carbon storage response. **b)** The relative contributions of individual NPP fluxes to the aggregated NPP response to eCO_2, including NPP responses of overstorey leaf (NPP_{ol}), twigs, barks and seeds (NPP_{other}), fine root (NPP_{froot}), and understorey aboveground (NPP_{ua}); **c)** The relative contributions of individual respiratory fluxes to the aggregated R response to eCO_2, including respiration responses of stem (R_{stem}), root (R_{root}), understorey aboveground (R_{ua}), growth (R_{grow}), and soil heterotroph (R_{hetero}); and **d)** The relative contributions of individual change in carbon storage to the aggregated ΔC_{pools} response to eCO_2, including changes in pool of stem (ΔC_{stem}), understorey aboveground (ΔC_{ua}), fine root (ΔC_{froot}), leaf litter (ΔC_{lit}), and soil (ΔC_{soil}). Variables with an absolute mean CO_2 effect of < 5 g C m^{-2} yr^{-1} are not reported in the bar chart for better visual clarification. Individual CO_2 responses are reported in Extended Data Figure 5. Each color represents the CO_2 response of a flux variable, the point indicates the net sum of all variables for a column, and the grey error bar represents one standard deviation of the estimated column sum at the plot-level (see Methods). The CO_2 effect is estimated using a linear mixed-model analysis with plot-specific pre-treatment leaf area index as a covariate to account for pre-existing differences (see Methods). The non-normalized response is provided in Extended Data Figure 4, which generally agrees with findings present in this figure, but with larger uncertainty.

Figure 3. Estimates of net ecosystem production (NEP) under ambient and elevated CO_2 treatment at EucFACE. Positive values indicate ecosystem net carbon uptake by the ecosystem. "In - Out" calculates NEP based on the difference between total influxes and total outfluxes. "NPP - R_{hetero}" calculates NEP based on the difference between net primary production (NPP) and heterotrophic respiration (R_{hetero}). "ΔC_{pools}" derives NEP based on incremental changes in all ecosystem carbon pools. Colored bars indicate treatment means based on each method (n=3), with blue representing ambient and red representing elevated CO_2 treatment. Individual dots are plot-level NEP, derived based on different methods (see Methods). Values are normalized by a linear mixed-model with plot-specific pre-treatment leaf area index as a covariate to account for pre-existing differences. Horizontal dotted line indicates NEP equals zero. The inset figure includes an inferred production allocation flux to mycorrhizal fungi (NPP_{myco}) based on data assimilation (Methods), which affected NEP estimates based on the NPP – R_{hetero} method only.

Extended Data Table 1. Definition and data availability of variables. Data availability includes start and end year of data included in this study. Time points indicate the number of data collections over the available data period. Within plot sub-replicate indicate the number of replicates within each treatment plot. The detailed methods for estimating each variable is provided in the Method section.

Variable		Data coverage			
Name	**Symbol**	**Start year**	**End year**	**Time points**	**Within plot sub-replicate ($plot^{-1}$)**
Specific Leaf Area	SLA	2013	2016	50	3
Leaf Area Index	LAI	2012	2016	303	1
Soil bulk density	BK	2017	2017	2	3
Diameter at breast height	DBH	2013	2016	4	Individual tree
Overstorey leaf pool	C_{ol}	2012	2016	303	1
Understorey aboveground pool	C_{ua}	2015	2016	16	4
Overstorey stem C pool	C_{stem}	2013	2016	4	Individual tree
Fine root C pool	C_{froot}	2014	2016	7	4
Intermediate root C pool	C_{iroot}	2014	2016	7	4
Coarse root C pool	C_{croot}	2013	2016	4	Individual tree
Forest floor leaf litter C pool	C_{lit}	2013	2016	46	-
Microbial C pool	C_{micr}	2012	2015	15	4
Soil C pool	C_{soil}	2012	2014	11	4

Mycorrhizal C pool	C_{myco}	2015	2015	3	-
Insect C pool (aerial)	C_{ins}	2013	2016	43	8
Insect C pool (understorey)	C_{ins}	2014	2015	5	2
Overstorey gross primary production	GPP_o	2013	2016	Annual	1
Understorey gross primary production	GPP_u	2013	2016	Annual	1
Overstorey leaf respiration	R_{ol}	2013	2016	Annual	1
Understorey leaf respiration	R_{ua}	2013	2016	Annual	1
Stem respiration	R_{stem}	2012	2016	Daily	3
Root respiration	R_{root}	2012	2015	Daily	-
Methane net flux	CH_4	2013	2016	35	7
Volatile C emission flux	VC	2013	2016	Daily	1
Insect herbivore respiration	R_{ins}	2012	2014	22	-
Dissolved organic C loss flux	DOC	2012	2014	12	4
Soil respiration	R_{soil}	2012	2015	Daily	8
Growth respiration	R_{grow}	2012	2016	Annual	1
Overstorey leaf net primary production	NPP_{ol}	2012	2016	49	8
Stem net primary production	NPP_{stem}	2012	2016	4	Individual tree
Fine root net primary production	NPP_{froot}	2014	2016	6	4
Intermediate root net primary production	NPP_{iroot}	2014	2016	6	4

Coarse root net primary production	NPP_{croot}	2012	2016	4	Individual tree
Other net primary production (sum of twigs, bark, seeds)	NPP_{other}	2012	2016	49	8
Twig net primary production	NPP_{twig}	2012	2016	49	8
Bark net primary production	NPP_{bark}	2012	2016	49	8
Seed net primary production	NPP_{seed}	2012	2016	49	8
Understorey aboveground net primary production	NPP_{ua}	2015	2016	3	4
Frass production	Frass	2012	2014	22	8
Heterotrophic respiration	R_{hetero}	2012	2016	Daily	8
Overstorey leaf insect consumption flux	NPP_{ins}	2012	2014	22	-

986

Extended Data Table 2. Carbon (C) fraction used to convert from biomass into C content.

Variable	Symbol	Mean value	Data source
C fraction of overstorey leaf pool	f_{ol}	0.5	EucFACE data
C fraction of understorey aboveground pool	f_{ua}	0.456	EucFACE data
C fraction of stem pool	f_{stem}	0.445 (ambient plots) 0.448 (elevated plots)	EucFACE data
C fraction of coarse root pool	f_{croot}	0.445 (ambient plots) 0.448 (elevated plots)	Assumed the same as f_{stem}
C fraction of fine root pool	f_{froot}	0.40 (ambient plots) 0.42 (elevated plots)	EucFACE data
C fraction of intermediate root pool	F_{iroot}	0.40 (ambient plots) 0.42 (elevated plots)	Assumed the same as f_{froot}
C fraction of overstorey leaflitter pool	f_{lit}	0.5	EucFACE data
C fraction of aboveground insect pool	f_{ins}	0.5	Ref 49
C fraction of frass production	f_{frass}	0.53	EucFACE data
C fraction of microbial pool	f_{micr}	0.534 (ambient plots) 0.493 (elevated plots)	EucFACE data
C fraction of mycorrhizal pool	f_{myco}	0.534 (ambient plots) 0.493 (elevated plots)	Assumed the same as f_{micr}
C fraction of soil pool	f_{soil}	0.016 (ambient plots) 0.017 (elevated plots)	EucFACE data
C fraction of twigs, barks and seeds production	f_{other}	0.5	Assumed

Extended Data Figure 1. The *Eucalyptus* Free Air Carbon dioxide Enrichment experiment facility (EucFACE). **a)** View of the forest and facility from above (photo credit: David S. Ellsworth), **b)** view of the understorey vegetation and infrastructure inside a plot (photo credit: Mingkai Jiang), and **c)** view from below of the canopy structure and the crane (photo credit: Mingkai Jiang).

Extended Data Figure 2. Mean annual temperature (MAT) and mean annual precipitation (MAP) for major forest biomes and a selected list of tree-based elevated CO_2 experiments. Gridded temperature and precipitation data were obtained from the Climate Research Unit (CRU) monthly dataset at 0.5 resolution[75]. Global biome boundaries and definitions were taken from Ref 76 and were spatially aggregated onto the CRU resolution, following Ref 77. The major forest biomes are defined as: tropical and subtropical moist broadleaf forests; tropical and subtropical dry broadleaf forests; tropical and subtropical coniferous forest; temperate broadleaf and mixed forests; temperate coniferous forests; boreal forests/taiga; and Mediterranean forests, woodlands, and scrub. The list of elevated CO_2 experiments includes 7 Free Air CO_2 Enrichment experiments (FACE) and a Whole-Tree Chamber experiment (WTC), namely: EucFACE, DukeFACE, ORNLFACE, AspenFACE, PopFACE, WebFACE, BiForFACE, and FlakalidenWTC. The site-specific climate, tree age and net primary production (NPP) under ambient CO_2 treatment were collected from Ref 3, 9, 10, 11, 78 and 79. The top inset figure compares global forest NPP against standing age using data collected from Ref 80. We included data with forest age < 500 years, and the NPP reported in Ref 80 included both overstorey and understorey. The bottom inset figure compares soil total nitrogen and labile phosphorus across the eCO_2 experiments. Soil total nitrogen was extracted from Ref 81 using spatial coordinates of each experiment, while soil labile phosphorus was spatially extracted from Ref 82. The two dotted lines indicates N:P ratios of 20:1 and 100:1, respectively.

Extended Data Figure 3. Estimates of (a and b) gross primary production (GPP) and (c and d) soil respiration (R_{soil}) based on different methods for both (a and c) ambient and (b and d) elevated CO_2 treatment at EucFACE. For estimates of GPP, we compared the model simulated total GPP of overstorey and understorey (GPP_o and GPP_u, respectively), with the sum of data-driven estimates of net primary production (NPP) and autotrophic respiration (R_a), which include NPP of overstorey leaf (NPP_{ol}), stem (NPP_{stem}), fine root (NPP_{froot}), intermediate root (NPP_{iroot}), coarse root (NPP_{croot}), twigs, barks and seeds (NPP_{other}), understorey aboveground (NPP_{ua}), leaf consumption by insects (NPP_{ins}), and respiratory fluxes of overstorey leaf (R_{ol}), stem (R_{stem}), root (R_{root}), understorey aboveground (R_{ua}), growth (R_{grow}), and volatile carbon emission (VC). For estimates of R_{soil}, we compared direct estimates of R_{soil} scaled up from soil chamber measurements, with the sum of litterfall and independent estimates of root respiration (Litter + R_{root}), assuming no net change in soil carbon stock over time. Here litterfall was inferred based on NPP of overstorey leaf (NPP_{ol}), fine root (NPP_{froot}), intermediate root (NPP_{iroot}), twigs, barks and seeds (NPP_{other}), understorey aboveground (NPP_{ua}), and frass production (Frass). These evaluations provide independent mass balance checks of the estimated ecosystem carbon budget. Each color represents a flux variable. Dotted point and vertical line represent treatment mean and standard deviation based on plot-level estimates of the aggregated flux (n=3). Values were normalized by a linear mixed-model with pre-treatment leaf area index as a covariate to account for pre-existing differences.

Extended Data Figure 4. The fate of additional carbon fixed under elevated CO_2 (eCO_2) in a mature forest ecosystem (non-normalized analysis case). a) Column **"**GPP" represents the total eCO_2 induced increase in overstorey and understorey gross primary production (GPP_o and GPP_u, respectively), column "NPP + R_a" represents the sum of net primary production and autotrophic respiration eCO_2 response, and column "R + ΔC_{pools}" represents the sum of ecosystem respiration and carbon storage eCO_2 response. **b)** The relative contributions of individual NPP fluxes to the aggregated NPP response to eCO_2, including overstorey leaf (NPP_{ol}), stem (NPP_{stem}), fine root (NPP_{froot}) and understorey aboveground (NPP_{ua}). **c)** The relative contributions of individual respiratory fluxes to the aggregated R response to eCO_2, including overstorey leaf (R_{ol}), stem (R_{stem}), root (R_{root}), understorey aboveground (R_{ua}), and heterotroph (R_{hetero}). **d)** The relative contributions of individual change in carbon storage to the aggregated ΔC_{pools} response to eCO_2, including stem (ΔC_{stem}), fine root (ΔC_{froot}), leaflitter (ΔC_{lit}), understorey aboveground (ΔC_{ua}), and soil (ΔC_{soil}). Variables with an average CO_2 effect of < 5 g C m^{-2} yr^{-1} were excluded from the figure for better visual clarification. Each color represents a flux variable, point indicates the net sum of all variables for a column, and the grey confidence interval represents plot-level standard deviation (n=3) of the estimated column sum.

Extended Data Figure 5. CO_2 treatment effect (g C m^{-2} yr^{-1}) for all ecosystem fluxes at EucFACE. a) The CO_2 response of gross ecosystem carbon uptake, including gross primary production of overstorey (GPP_o) and understorey (GPP_u), and soil methane uptake (CH_4). **b)** The eCO_2 response of annual incremental change in carbon pool (ΔC_{pools}), including overstorey leaf (ΔC_{ol}), stem (ΔC_{stem}), coarse root (ΔC_{croot}), fine root (ΔC_{froot}), intermediate root (ΔC_{iroot}), understorey aboveground (ΔC_{ua}), leaf litter (ΔC_{lit}), soil (ΔC_{soil}), microbe (ΔC_{micr}), aboveground insect (ΔC_{ins}), and mycorrhizae (ΔC_{myco}). **c)** The eCO_2 response of net primary production (NPP), including overstorey leaf (NPP_{ol}), stem (NPP_{stem}), coarse root (NPP_{croot}), fine root (NPP_{froot}), intermediate root (NPP_{iroot}), understorey aboveground (NPP_{ua}), twigs, barks and seeds (NPP_{other}), and leaf insect consumption (NPP_{ins}). **d)** The eCO_2 response of ecosystem respiration (R) and other out-going flux, including respiration fluxes of overstorey leaf (R_{ol}), stem (R_{stem}), root (R_{root}), understorey aboveground (R_{ua}), growth (R_{grow}), insect (R_{ins}), heterotroph (R_{hetero}), and soil (R_{soil}), and volatile carbon emission (VC) and dissolved organic carbon leaching (DOC). Dots and grey bars represent means and standard deviations of the CO_2 treatment difference, predicted by a linear mixed-model with plot-specific pre-treatment leaf area index as a covariate. Red dots indicate negative means and blue dots indicate positive means. Dashed lines indicate change of scale along the x-axis.

Extended Data Figure 6. Estimates of incremental change in carbon pool averaged over the experimental period under ambient (aCO_2) and elevated CO_2 (eCO_2) treatment effect at EucFACE (ΔC_{pools}, g C m^{-2} yr^{-1}). The ΔC_{pools} variables are overstorey leaf (ΔC_{ol}), stem (ΔC_{stem}), coarse root (ΔC_{croot}), fine root (ΔC_{froot}), intermediate root (ΔC_{iroot}), understorey aboveground (ΔC_{ua}), leaf litter (ΔC_{lit}), soil (ΔC_{soil}), microbe (ΔC_{micr}), aboveground insect (ΔC_{ins}), and mycorrhizae (ΔC_{myco}). Colored bars and black lines represent means and standard deviations for each treatment, with blue represents aCO_2 and red represents eCO_2 treatment. Dashed lines indicate change of scale along the x-axis.

Extended Data Figure 7. Fitted carbon cycle parameters to trace the fate of the additional carbon under elevated CO_2 at EucFACE. Parameters were estimated by Markov Chain Monte Carlo (MCMC) fitting algorithm, assuming a simplified carbon cycle framework based on data collected from EucFACE. Details of the MCMC approach can be found in the Methods. Plot-level gross primary production (GPP), autotrophic respiration (R_a), heterotrophic respiration (R_{hetero}), carbon pools of leaf (C'_{leaf}), wood (C'_{wood}), root (C'_{root}), mycorrhizae (C'_{myco}), microbe (C'_{micr}), and soil (C'_{soil}), and the corresponding change in pools were used to constrain the model fitting. Net primary production (NPP) was derived as the difference of GPP and R_a. Carbon use efficiency (CUE') was calculated as NPP/GPP; it differs from the value given in the main text owing to the contribution of NPP allocated to mycorrhizae (NPP_{myco}). We fitted two carbon pools (C'_{aglit} and C'_{bglit}), four allocation coefficients (a_{leaf}, a_{wood}, a_{root}, and a_{myco}), six turnover rates (τ_{leaf}, τ_{root}, τ_{myco}, τ_{bglit}, τ_{micr}, and τ_{soil}), and three fractional coefficients (f'_{aglit}, f'_{bglit}, and f'_{micr}) using MCMC algorithm. The fractional coefficients indicate the fraction of carbon leaving one pool that enters the subsequent pool, with the remainder respired as R_{hetero}.

Extended Data Figure 8. Data-model intercomparison of some key carbon cycle parameters, under ambient (aCO_2) and elevated CO_2 (eCO_2). Parameters include: **a)** allocation coefficients to leaf, wood, root and other, **b)** turnover rates of leaf, root, aboveground litter (Aglit), belowground litter (Bglit), and **c)** turnover rate of soil. Models include: Community Atmosphere Biosphere Land Exchange (CABL), Community Land Model 4 (CLM4), Community Land Model with a phosphorus component (CLMP), Generic Decomposition And Yield (GDAY), Lund-Potsdam-Jena General Ecosystem Simulator (LPJX), Orchidee-C-N (OCNX), and Sheffield Dynamic Global Vegetation Model (SDVM). The model output was generated as part of the model ensemble predictions made in advance of the experiment reported in Ref 17 for EucFACE. Data-based uncertainties were estimated using the Markov Chain Monte Carlo data assimilation algorithm, with error bars indicating one standard deviation. Allocation to other in the data refers to the allocation to mycorrhizal production, whereas it refers to the allocation to reproductive carbon pool in some models.

Figures

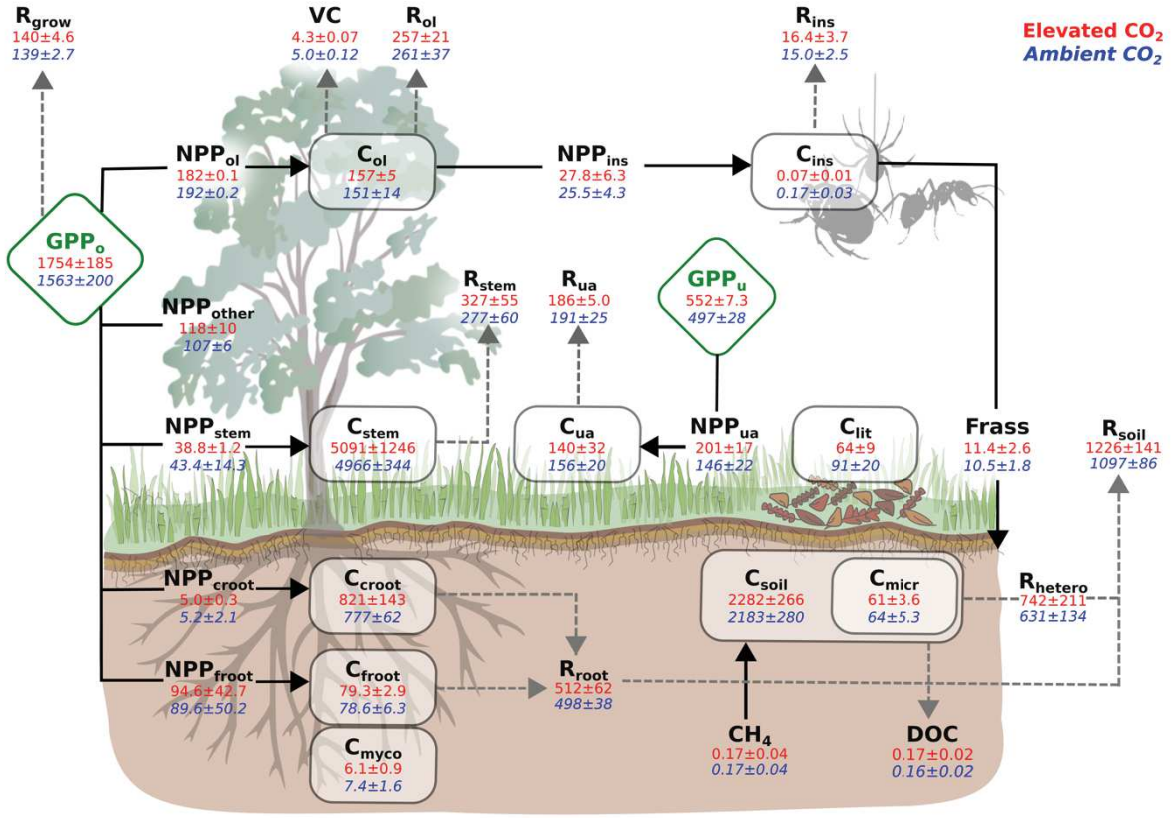

Figure 1. A comprehensive carbon budget under ambient and elevated CO_2 treatment in a mature forest ecosystem. Diamond boxes are gross primary production for overstorey (GPP_o) and understorey (GPP_u), respectively. Squared boxes are carbon stocks (gCm^{-2}), including overstorey leaf (C_{ol}), stem (C_{stem}), coarse root (C_{croot}), fineroot (C_{froot}), understorey aboveground (C_{ua}), leaf litter (C_{lit}), soil (C_{soil}), microbe (C_{micr}), aboveground insect (C_{ins}), and mycorrhizae (C_{myco}). Unboxed variables are carbon fluxes ($gCm^{-2}yr^{-1}$), including net primary production of overstorey leaf (NPP_{ol}), stem (NPP_{stem}), coarse root (NPP_{croot}), fineroot (NPP_{froot}), and understorey aboveground (NPP_{ua}), overstorey leaf consumption by insects (NPP_{ins}), respiration fluxes of overstorey leaf (R_{ol}), stem (R_{stem}), root (R_{root}), understorey aboveground (R_{ua}), growth (R_{grow}), insect (R_{ins}), heterotroph (R_{hetero}), and soil (R_{soil}), and volatile carbon emission (VC), frass production (Frass), dissolved organic carbon (DOC), and soil methane net

775 uptake (CH_4). Solid arrow lines are fluxes entering a pool, dotted arrow lines are fluxes leaving
776 a pool. Blue italic values are means ± one standard deviation of the ambient CO_2 treatment
777 (n=3), whereas red values are means ± one standard deviation of the elevated CO_2 treatment
778 (n=3). All values are normalized by a linear mixed-model with plot-specific pre-treatment leaf
779 area index as a covariate to account for pre-existing differences. Summary of variable
780 definitions and data availability is provided in Extended Data Table 1.

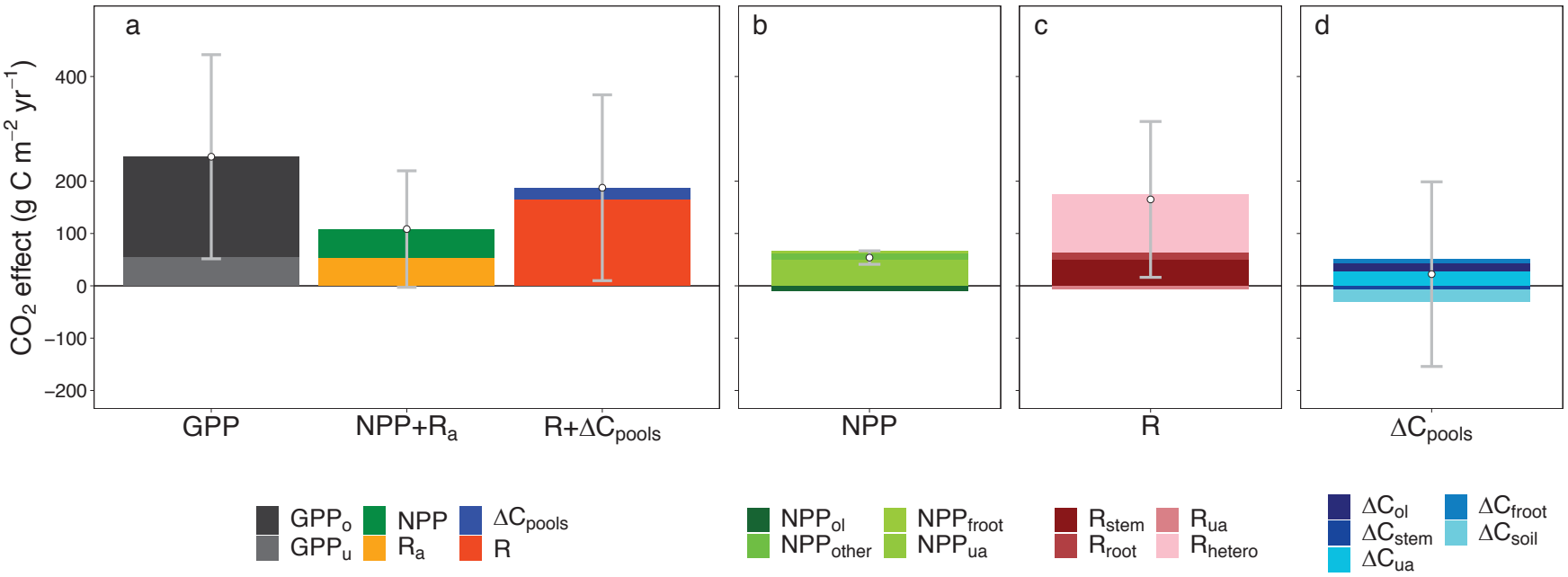

Figure 2. The fate of additional carbon fixed under elevated CO_2 (eCO_2) in a mature forest ecosystem. a) Column **"**GPP" represents the total eCO_2-induced increases in overstorey and understorey gross primary production (GPP_o and GPP_u, respectively), "NPP + R_a" represents the sum of net primary production and autotrophic respiration response, "R + ΔC_{pools}" represents the sum of ecosystem respiration and carbon storage response. **b)** The relative contributions of individual NPP fluxes to the aggregated NPP response to eCO_2, including NPP responses of overstorey leaf (NPP_{ol}), twigs, barks and seeds (NPP_{other}), fineroot (NPP_{froot}), and understorey aboveground (NPP_{ua}); **c)** The relative contributions of individual respiratory fluxes to the aggregated R response to eCO_2, including respiration responses of stem (R_{stem}), root (R_{root}), understorey aboveground

789 (R_{ua}), and soil heterotroph (R_{hetero}); and **d)** The relative contributions of individual change in carbon storage to the aggregated ΔC_{pools} response to
790 eCO_2, including changes in pool of overstorey leaf (ΔC_{ol}), stem (ΔC_{stem}), understorey aboveground (ΔC_{ua}), fineroot (ΔC_{froot}), and soil (ΔC_{soil}).
791 Variables with an absolute mean CO_2 effect of < 5 $gCm^{-2}yr^{-1}$ are excluded from the figure for better visual clarification. Individual CO_2 responses
792 are reported in Extended Data Figure 4. Each color represents the CO_2 response of a flux variable, point indicates the net sum of all variables for
793 a column, and the grey error bar represents one standard deviation of the estimated column sum at the plot-level (see Methods). The CO_2 effect is
794 estimated using a linear mixed-model analysis with plot-specific pre-treatment leaf area index as a covariate to account for pre-existing differences
795 (see Methods). The un-normalized response is provided in Extended Data Figure 3, which generally agrees with findings present in this figure, but
796 with less statistical precision.

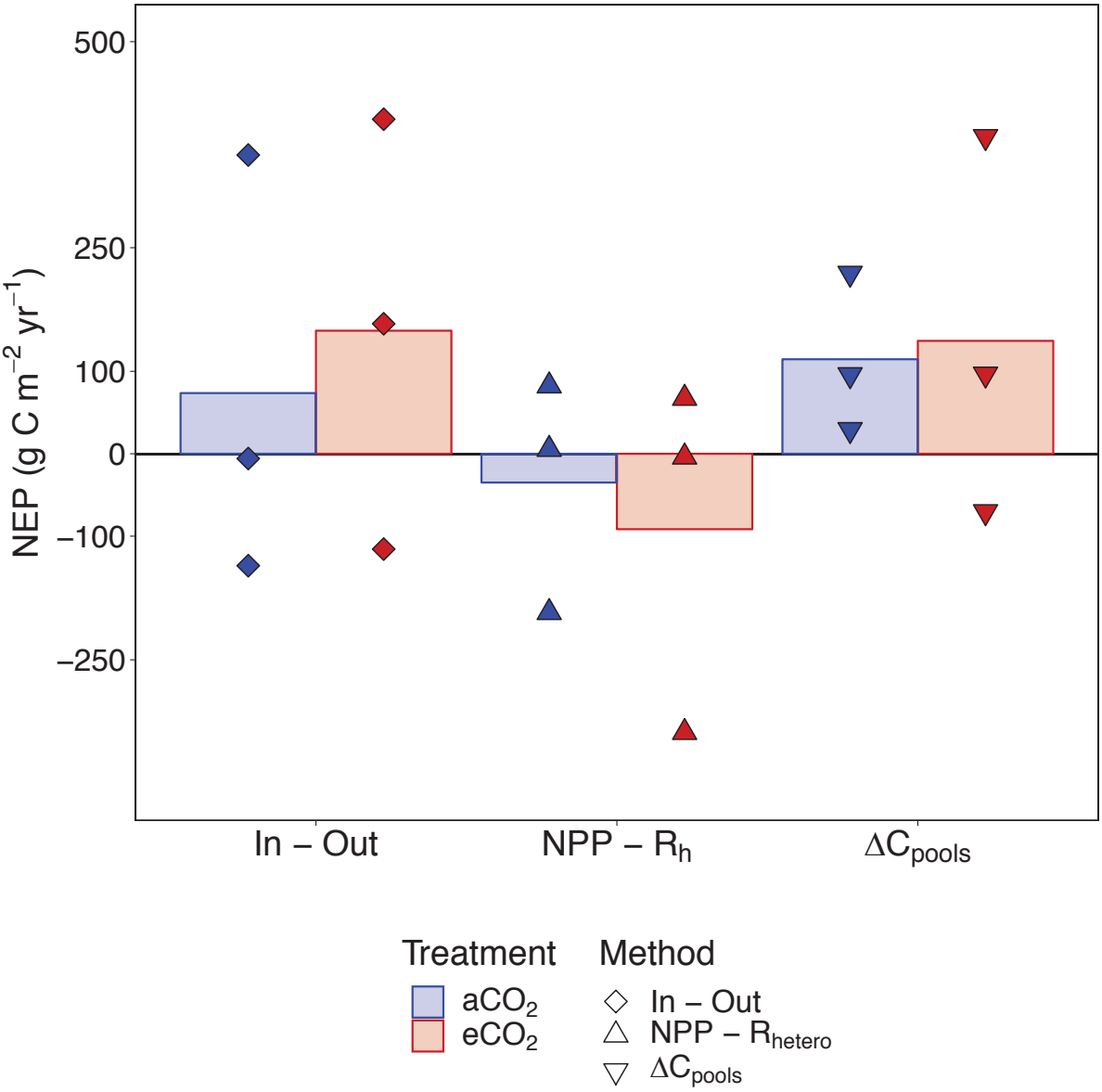

Figure 3. Estimates of net ecosystem production (NEP) under ambient and elevated CO_2 treatment at EucFACE. Positive values indicate ecosystem net carbon uptake by the ecosystem. "In - Out" calculates NEP based on the difference between total influxes and total outfluxes. "NPP - R_{hetero}" calculates NEP based on the difference between net primary production (NPP) and heterotrophic respiration (R_{hetero}). "ΔC_{pools}" derives NEP based on incremental changes in all ecosystem carbon pools. Colored bars indicate treatment means based on each method (n=3), with blue representing ambient and red representing elevated CO_2

806 treatment. Individual dots are plot-level NEP, derived based on different methods (see
807 Methods). Values are normalized by a linear mixed-model with plot-specific pre-treatment leaf
808 area index as a covariate to account for pre-existing differences. Horizontal dotted line indicates
809 NEP equals zero.

Extended Data Table 1. Definition and data availability of variables. Data availability includes start and end year of data included in this study. Time points indicate the number of data collections over the available data period. Within plot sub-replicate indicate the number of replicates within each treatment plot. The detailed methods for estimating each variable is provided in the Method section.

Variable		**Data coverage**			
Name	**Symbol**	**Start year**	**End year**	**Time points**	**Within plot sub-replicate ($plot^{-1}$)**
Specific Leaf Area	SLA	2013	2016	50	3
Leaf Area Index	LAI	2012	2016	303	1
Soil bulk density	BK	2017	2017	2	3
Diameter at breast height	DBH	2013	2016	4	Individual tree
Overstorey leaf pool	C_{ol}	2012	2016	303	1
Understorey aboveground pool	C_{ua}	2015	2016	16	4
Overstorey stem C pool	C_{stem}	2013	2016	4	Individual tree
Fine root C pool	C_{froot}	2014	2016	6	4
Coarse root C pool	C_{croot}	2013	2016	4	Individual tree
Forest floor leaf litter C pool	C_{lit}	2013	2016	46	-
Microbial C pool	C_{micr}	2012	2015	15	4
Soil C pool	C_{soil}	2012	2014	11	4

Mycorrhizal C pool	C_{myco}	2015	2015	3	-
Insect C pool (aeriel)	C_{ins}	2013	2016	43	8
Insect C pool (ground dwelling)	C_{ins}	2013	2015	5	4
Overstorey gross primary production	GPP_o	2013	2016	Annual	1
Understorey gross primary production	GPP_u	2013	2016	Annual	1
Overstorey leaf respiration	R_{ol}	2013	2016	Annual	1
Understorey leaf respiration	R_{ua}	2013	2016	Annual	1
Stem respiration	R_{stem}	2012	2016	Daily	3
Root respiration	R_{root}	2012	2015	Daily	-
Methane net flux	CH_4	2013	2016	35	7
Volatile C emission flux	VC	2013	2016	Daily	1
Insect herbivore respiration	R_{ins}	2012	2014	22	-
Dissolved organic C loss flux	DOC	2012	2014	12	4
Soil respiration	R_{soil}	2012	2015	Daily	8
Growth respiration	R_{grow}	2012	2016	Annual	1
Overstorey leaf net primary production	NPP_{ol}	2012	2016	49	8
Stem net primary production	NPP_{stem}	2012	2016	4	Individual tree

Fine root net primary production	NPP_{froot}	2014	2016	5	4
Coarse root net primary production	NPP_{croot}	2012	2016	4	Individual tree
Other net primary production (sum of twigs, bark, seeds)	NPP_{other}	2012	2016	49	8
Twig net primary production	NPP_{twig}	2012	2016	49	8
Bark net primary production	NPP_{bark}	2012	2016	49	8
Seed net primary production	NPP_{seed}	2012	2016	49	8
Understorey aboveground net primary production	NPP_{ua}	2015	2016	3	4
Frass production	Frass	2012	2014	22	8
Heterotrophic respiration	R_{hetero}	2012	2016	Daily	8
Overstorey leaf insect consumption flux	NPP_{ins}	2012	2014	22	-

815

Extended Data Table 2. Carbon (C) fraction used to convert from biomass into C content.

Variable	Symbol	Mean value	Data source
C fraction of overstorey leaf pool	f_{ol}	0.5	EucFACE data
C fraction of understorey aboveground pool	f_{ua}	0.456	EucFACE data
C fraction of stem pool	f_{stem}	0.445 (ambient plots) 0.448 (elevated plots)	EucFACE data
C fraction of coarse root pool	f_{croot}	0.445 (ambient plots) 0.448 (elevated plots)	Assumed the same as f_{stem}
C fraction of fine root pool	f_{froot}	0.40 (ambient plots) 0.42 (elevated plots)	EucFACE data
C fraction of overstorey leaflitter pool	f_{lit}	0.5	EucFACE data
C fraction of aboveground insect pool	f_{ins}	0.5	Ref 48
C fraction of frass production	f_{frass}	0.53	EucFACE data
C fraction of microbial pool	f_{micr}	0.534 (ambient plots) 0.493 (elevated plots)	EucFACE data

C fraction of mycorrhizal pool	f_{myco}	0.534 (ambient plots) 0.493 (elevated plots)	Assumed the same as f_{micr}
C fraction of soil pool	f_{soil}	0.016 (ambient plots) 0.017 (elevated plots)	EucFACE data
C fraction of twigs, barks and seeds production	f_{other}	0.5	Assumed

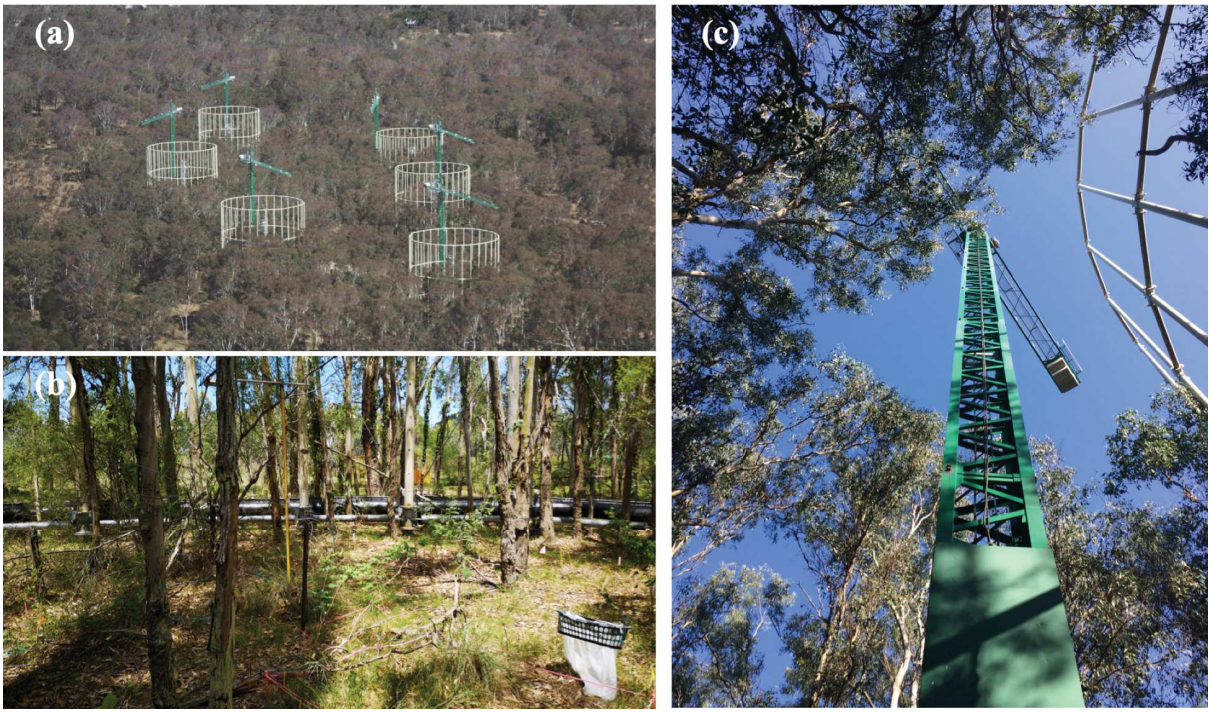

Extended Data Figure 1. The *Eucalyptus* free air carbon dioxide enrichment experiment facility (EucFACE). **a)** A spatial overview of the forest and the facility (photo credit: David S. Ellsworth), **b)** an overview of the understorey vegetation and infrastructure inside a plot (photo credit: Mingkai Jiang), and **c)** a bottom-up look of the canopy structure and the crane (photo credit: Mingkai Jiang).

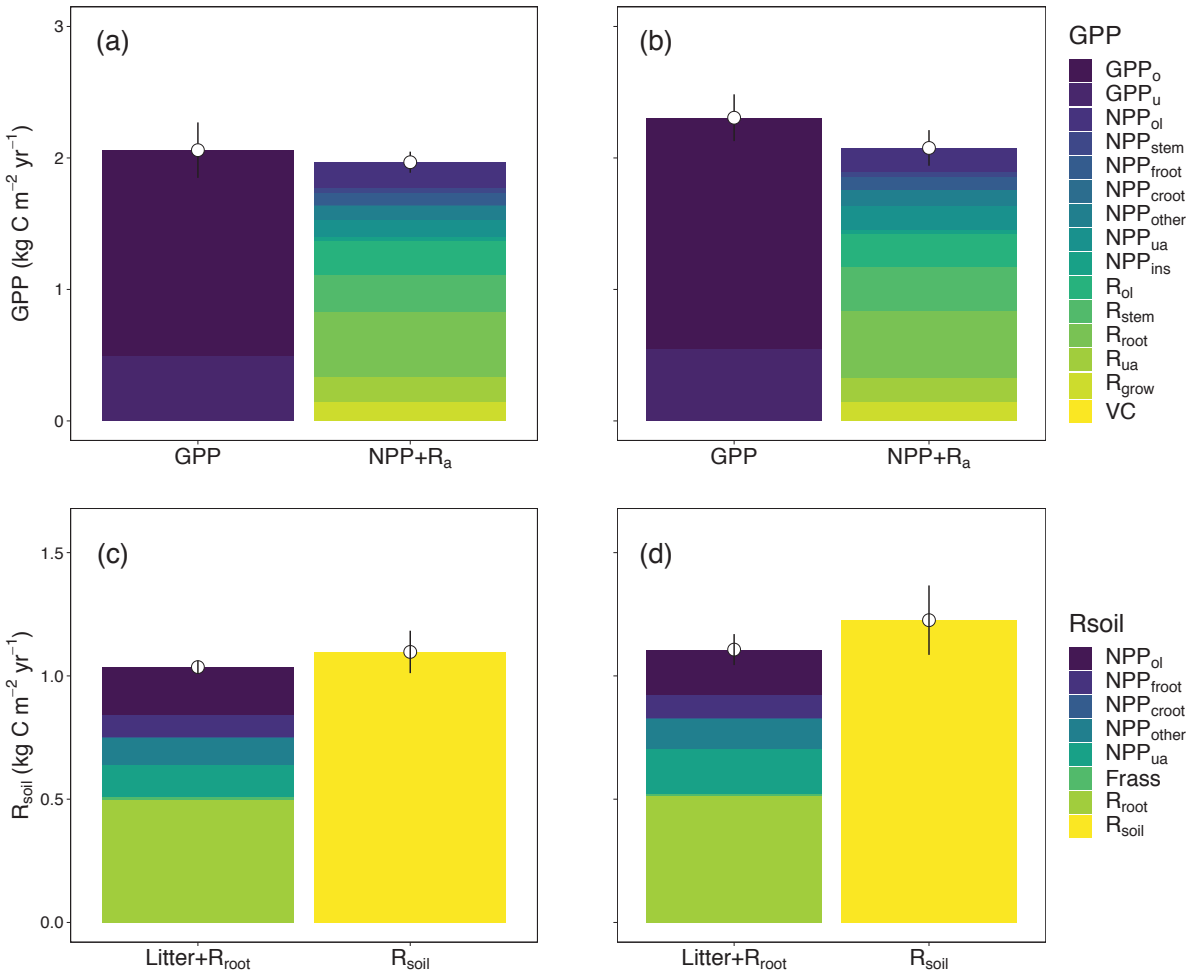

Extended Data Figure 2. Estimates of (a and b) gross primary production (GPP) and (c and d) soil respiration (R_{soil}) based on different methods for both (a and c) ambient and (b and d) elevated CO_2 treatment at EucFACE. For estimates of GPP, we compared the model simulated total GPP of overstorey and understorey (GPP_o and GPP_u, respectively), with the sum of data-driven estimates of net primary production (NPP) and autotrophic respiration (R_a), which include NPP of overstorey leaf (NPP_{ol}), stem (NPP_{stem}), fineroot (NPP_{froot}), coarse root (NPP_{croot}), twigs, barks and seeds (NPP_{other}), understorey aboveground (NPP_{ua}), leaf consumption by insects (NPP_{ins}), and respiratory fluxes of overstorey leaf (R_{ol}), stem (R_{stem}), root (R_{root}), understorey aboveground (R_{ua}), growth (R_{grow}), and volatile carbon emission (VC). For estimates of R_{soil}, we compared direct estimates of R_{soil} scaled up from soil chamber

measurements, with the sum of litterfall and independent estimates of root respiration (Litter + R_{root}), assuming no net change in soil carbon stock over time. Here litterfall was inferred based on NPP of overstorey leaf (NPP_{ol}), fineroot (NPP_{froot}), coarse root (NPP_{croot}), twigs, barks and seeds (NPP_{other}), understorey aboveground (NPP_{ua}), and frass production (Frass). These evaluations provide independent mass balance checks of the estimated ecosystem carbon budget. Each color represents a flux variable. Dotted point and vertical line represent treatment mean and standard deviation based on plot-level estimates of the aggregated flux (n=3). Values were normalized by a linear mixed-model with pre-treatment leaf area index as a covariate to account for pre-existing differences.

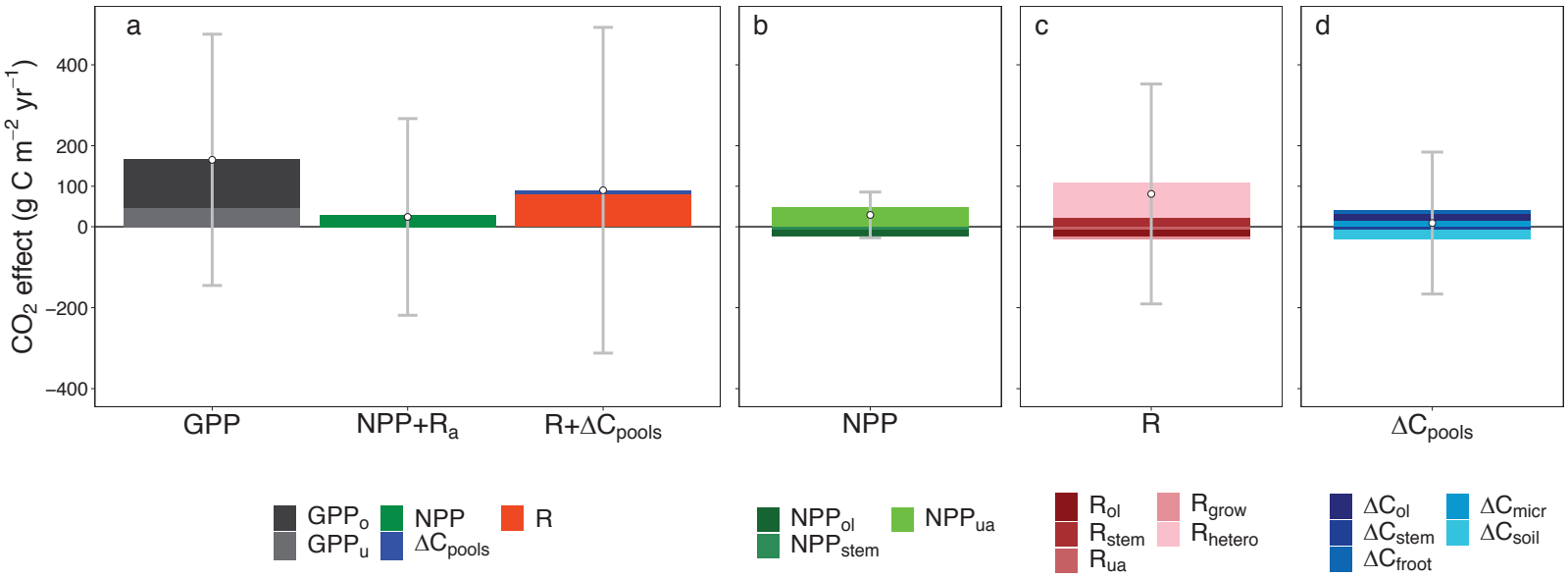

Extended Data Figure 3. The fate of additional carbon fixed under elevated CO_2 (eCO_2) in a mature forest ecosystem (non-normalized analysis case). a) Column **"**GPP" represents the total eCO_2 induced increase in overstorey and understorey gross primary production (GPP_o and GPP_u, respectively), column "NPP + R_a" represents the sum of net primary production and autotrophic respiration eCO_2 response, and column "R + ΔC_{pools}" represents the sum of ecosystem respiration and carbon storage eCO_2 response. **b)** The relative contributions of individual NPP fluxes to the aggregated NPP response to eCO_2, including overstorey leaf (NPP_{ol}), stem (NPP_{stem}), and understorey aboveground (NPP_{ua}). **c)** The relative contributions of individual respiratory fluxes to the aggregated R response to eCO_2, including overstorey leaf (R_{ol}), stem (R_{stem}), understorey aboveground (R_{ua}), growth (R_{grow}), and heterotroph (R_{hetero}). **d)** The relative contributions of individual change in carbon storage to the aggregated ΔC_{pools} response to eCO_2, including overstorey leaf (ΔC_{ol}), stem (ΔC_{stem}), fineroot (ΔC_{froot}), microbe (ΔC_{micr}), and soil (ΔC_{soil}). Variables with an

855 average CO_2 effect of < 5 $gCm^{-2}yr^{-1}$ were excluded from the figure for better visual clarification. Each color represents a flux variable, point
856 indicates the net sum of all variables for a column, and the grey confidence interval represents plot-level standard deviation (n=3) of the estimated
857 column sum.

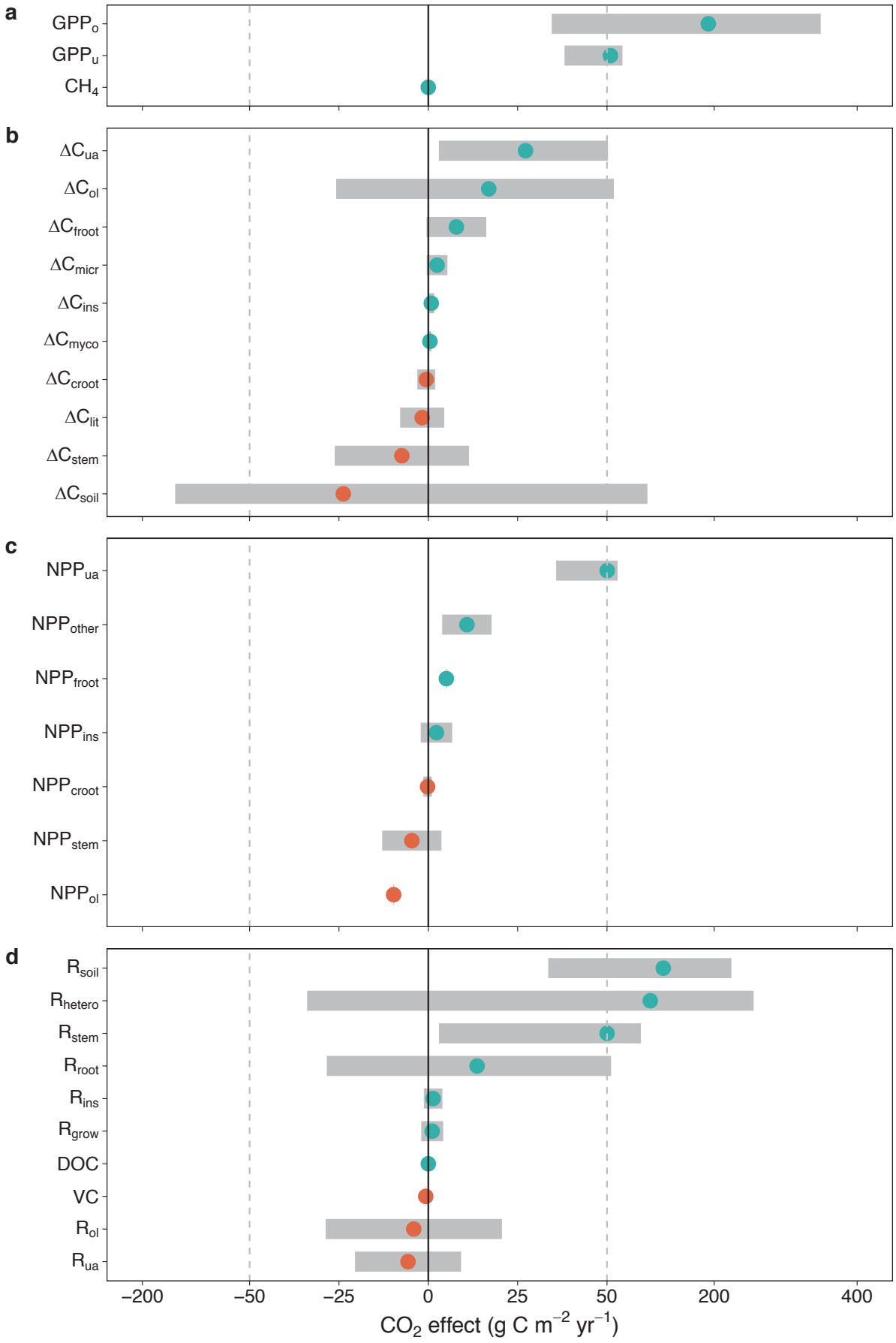
a
GPP$_o$
GPP$_u$
CH$_4$
b
ΔC$_{ua}$
ΔC$_{ol}$
ΔC$_{froot}$
ΔC$_{micr}$
ΔC$_{ins}$
ΔC$_{myco}$
ΔC$_{croot}$
ΔC$_{lit}$
ΔC$_{stem}$
ΔC$_{soil}$
c
NPP$_{ua}$
NPP$_{other}$
NPP$_{froot}$
NPP$_{ins}$
NPP$_{croot}$
NPP$_{stem}$
NPP$_{ol}$
d
R$_{soil}$
R$_{hetero}$
R$_{stem}$
R$_{root}$
R$_{ins}$
R$_{grow}$
DOC
VC
R$_{ol}$
R$_{ua}$
−200
−50
−25
0
25
50
200
400
CO$_2$ effect (g C m^{-2} yr^{-1})

Extended Data Figure 4. CO_2 treatment effect ($gCm^{-2}yr^{-1}$) for all ecosystem fluxes at EucFACE. a) The CO_2 response of gross ecosystem carbon uptake, including gross primary production of overstorey (GPP_o) and understorey (GPP_u), and soil methane uptake (CH_4). **b)** The eCO_2 response of annual incremental change in carbon pool (ΔC_{pools}), including overstorey leaf (ΔC_{ol}), stem (ΔC_{stem}), coarse root (ΔC_{croot}), fineroot (ΔC_{froot}), understorey aboveground (ΔC_{ua}), leaf litter (ΔC_{lit}), soil (ΔC_{soil}), microbe (ΔC_{micr}), aboveground insect (ΔC_{ins}), and mycorrhizae (ΔC_{myco}). **c)** The eCO_2 response of net primary production (NPP), including overstorey leaf (NPP_{ol}), stem (NPP_{stem}), coarse root (NPP_{croot}), fineroot (NPP_{froot}), understorey aboveground (NPP_{ua}), twigs, barks and seeds (NPP_{other}), and leaf insect consumption (NPP_{ins}). **d)** The eCO_2 response of ecosystem respiration (R) and other out-going flux, including respiration fluxes of overstorey leaf (R_{ol}), stem (R_{stem}), root (R_{root}), understorey aboveground (R_{ua}), growth (R_{grow}), insect (R_{ins}), heterotroph (R_{hetero}), and soil (R_{soil}), and volatile carbon emission (VC) and dissolved organic carbon leaching (DOC). Dots and grey bars represent means and standard deviations of the CO_2 treatment difference, predicted by a linear mixed-model with plot-specific pre-treatment leaf area index as a covariate. Orange dots indicate negative means and light green dots indicate positive means. Dashed lines indicate change of scale along the x-axis.